Muon-spin-relaxation studies of the alkali-fulleride superconductors

W. A. MacFarlane,* R. F. Kiefl, S. Dunsiger, J. E. Sonier, and J. Chakhalian
CIAR, Department of Physics and TRIUMF, University of British Columbia, Vancouver, British Columbia, Canada V6T 1Z1

J. E. Fischer
Materials Science Department and Laboratory for Research on the Structure of Matter, University of Pennsylvania, Philadelphia, Pennsylvania 19104-6272

T. Yildirim
University of Maryland, College Park, Maryland 20742
and National Institute of Standards and Technology, Gaithersburg, Maryland 20899

K. H. Chow
Department of Physics, Lehigh University, Bethlehem, Pennsylvania 18015
(Received 24 February 1998)

Muon-spin-rotation and relaxation experiments have been performed on the alkali-fulleride superconductors: Rb_3C_{60}, K_3C_{60}, Na_2CsC_{60}. A small fraction of the implanted muons form endohedral muonium ($Mu@C_{60}$), i.e., a μ^+e^- atom on the inside of the C_{60} cage. The presence of the unpaired electron on the muon greatly enhances the sensitivity of the muon to scattering from electronic excitations and the resulting muon-spin relaxation. The $1/T_1$ spin-relaxation rate of $Mu@C_{60}$ in a longitudinal field exhibits a Korringa-like temperature dependence in the normal state, and a small Hebel-Slichter coherence peak followed by activated temperature dependence well below T_c. In Rb_3C_{60} the coherence peak is strongly suppressed by a magnetic field which is well below H_{c2}. From the activated temperature dependence we obtain estimates of the superconducting energy gap. In addition, spin precession measurements of diamagnetic muons in the vortex state are used to estimate the magnetic penetration depth. In Na_2CsC_{60}, we find a quench rate dependence suggesting the existence of two low-temperature metallic phases, only one of which is superconducting. [S0163-1829(98)03725-4]

I. INTRODUCTION

Superconductivity in the alkali fullerides, A_3C_{60}, where A is an alkali-metal ion (or some mixture of several different alkali ions), poses interesting problems to the theoretical understanding of superconductivity generally. For example, these materials, due to their *molecular* nature, do not have the well-separated electron and phonon energy scales required for the validity of Migdal's theorem. A detailed discussion of the theoretical aspects of A_3C_{60} (abbreviated A_3) superconductivity can be found in the recent review of Gunnarsson[1] and references therein. It has generally been accepted that A_3 superconductivity is surprisingly of a rather conventional nature, i.e., phonon-mediated s-wave BCS; however, the reported fundamental parameters of superconductivity (such as the magnetic penetration depth λ, energy gap 2Δ, coherence length ξ) in these systems vary widely. While some of this variation can undoubtedly be explained by differences in sample quality in these materials which are difficult both to synthesize and to handle (the former because of the slow diffusion process of intercalation, and the latter because of their extreme air sensitivity), there remain significant discrepancies between results obtained using different techniques. Thus, in order to guide theoretical understanding of the unusual aspects of alkali-fulleride superconductivity, it is necessary to determine these parameters accurately as well as explain the origin of the discrepancies between various methods.

So far, all of the A_3 superconductors are extreme type-II, i.e., $\lambda \gg \xi$. Values of the critical fields, λ and ξ, from a wide variety of experiments can be found in the recent review by Buntar and Weber.[2] More recently, values of these parameters inferred from magnetization measurements of single crystals have been reported by Chu and McHenry,[3] who find the low-temperature values $\lambda \approx 1100$ Å and $\xi \approx 30$ Å. Köller *et al.*,[4] have measured the low-temperature energy gap via optical and tunneling spectroscopy and find that $2\Delta/kT_c = 4.2(2)$, i.e., the coupling is not in the weak limit where $2\Delta/kT_c = 3.76$. A detailed review of many experimental results can be found in the article of Ramirez.[5]

In this paper we report the results of muon-spin-rotation and relaxation experiments on three A_3 superconductors: Rb_3C_{60}, K_3C_{60}, and Na_2CsC_{60}. These three ionic fulleride salts are based on an fcc lattice of C_{60}^{3-} ions with the alkali ions adopting interstitial sites. The large Rb^+ and K^+ ions hinder rotation of the balls, and the C_{60}^{3-} ions form an fcc merohedrally disordered glass (space group $Fm\bar{3}m$). Freezing of the orientational dynamics of the C_{60}^{3-} ions in $Fm\bar{3}m$ materials has been studied by NMR.[6] The small size of the Na^+ allows the C_{60}^{3-} to adopt optimal orientations in a primitive cubic lattice[7] (space group $Pa\bar{3}$). However, very recently it has been found[8] that in Na_2Rb, this cubic phase is in fact metastable, with the equilibrium phase having polymerized C_{60}^{3-} ions. The tendency for polymerization of C_{60} in the

solid phase is well established, for example, the photopolymerization[9] in pure C_{60}, the cubic/orthorhombic structural phase transition[10,11] in A_1C_{60}, and the polymerization of Na_2AC_{60} under pressure.[12] Polymeric AC_{60} (for A = Rb or Cs) exhibits interesting electronic properties[10] such as apparent one-dimensionality and a low-temperature metal-magnetic insulator transition. On the other hand, for A=K, the behavior of the polymeric phase appears to be $3d$ metallic. It has been suggested[12] that the polymers in Na_2A are superconducting, but recent results in Na_2Rb (Ref. 8) indicate that they are not. It is clearly of considerable interest to firmly establish the properties of the polymeric structures in Na_2A both in their relation to the other metallic C_{60} polymers and the nonpolymeric fulleride superconductors.

Much information about the electronic and magnetic properties of solids can be obtained from magnetic resonance techniques using electrons, spin-bearing nuclei, or positive muons. Muon spin rotation is well known for its ability to measure the internal magnetic field distribution of the vortex state of type-II superconductors, and hence the characteristic parameters determining that distribution (λ and in some cases to a lesser degree ξ). Measurement of λ constitutes a measure of the superconducting electron density n_s via

$$\lambda^2 = m^*/\mu_0 e^2 n_s , \tag{1.1}$$

where m^* is the effective electron mass of the superconducting electrons, μ_0 is the vacuum permeability, and e is the electron charge. With respect to muons, A_3 superconductors are very unusual since a small fraction of the injected muons form a paramagnetic hydrogenlike atom called muonium (Mu) which is trapped within the C_{60} cage. In typical metals, screening of the μ^+ Coulomb potential by conduction electrons eliminates such a state. Currently the endohedral muonium Mu@C_{60} in the metallic alkali fullerides is the only known example of a paramagnetic muon state in a metal. The presence of the bound electron moment enhances the spin-relaxation rate (analogous to NMR T_1 relaxation) enormously ($\times 10^5$ at 1.5 T) over the rate expected for diamagnetic muons or the nuclei used in NMR experiments. The Mu spin relaxation is caused by spin exchange with the conduction electrons, and thus the temperature and field dependence of the relaxation rate yields information about the electronic excitation spectrum. Hence we are able to extract complementary information about the superconducting ground state, through $\lambda(n_s)$, and about its excitations through the T_1 relaxation.

II. EXPERIMENTAL

The experiments described in this paper were conducted on the $M15$ and $M20$ beamlines at TRIUMF, which provide high intensity beams of $\sim$100% spin polarized positive muons produced from the decay of pions at rest on the surface of a production target. The kinetic energy of such ''surface'' muons ($\sim$4.1 MeV) gives them a mean stopping range of 140 mg/cm^2; consequently, μSR is essentially a bulk probe.

One can follow the spin polarization of an ensemble of implanted muons via detection of their high-energy decay positrons which, due to the asymmetry of the weak decay of the muon, are emitted preferentially along the direction of the muon spin at the time of decay. The entry of a muon into the sample and its decay positron are detected with fast plastic scintillation detectors. The muon detector is thin enough ($\approx$0.25 mm) that muons will pass through it. Typically there is an array of between 1 and 4 positron detectors around the sample. The histogram of the time differences between muon implantation and decay positron detection in counter i is of the form:

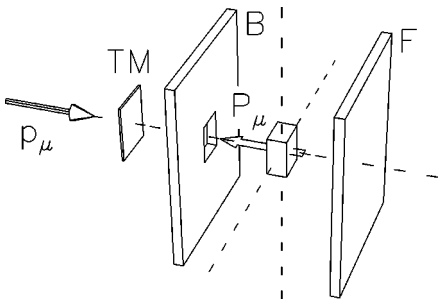

FIG. 1. Schematic of a longitudinal field μSR experiment showing the sample and three counters. Muons of momentum $\mathbf{p}_\mu$ and spin polarization $\mathbf{P}_\mu$ (antialigned) pass through the thin muon (TM) counter and the aperture in the B counter. The decay positrons are detected via the backward (B) and forward (F) counters. The magnetic field is directed parallel to $\mathbf{P}_\mu$.

$$N_i(t) = N_{i0} e^{-t/\tau_\mu}[1 + A_i \mathbf{P}_\mu(t)\cdot\hat{i}] + B_i , \tag{2.1}$$

where N_{i0} is an overall normalization, B_i is a time-independent background, A_i is the experimental asymmetry typically in the range 0.2–0.3, $\hat{i}$ is a unit vector along the direction joining the center of the sample to the center of the solid angle subtended by the counter i, $\tau_\mu \approx 2.2$ μs is the muon lifetime which sets the practical upper limit for the time scale of observable variations in $\mathbf{P}_\mu(t)$, the muon spin polarization. Through a variety of methods, one extracts $A_i\mathbf{P}_\mu(t)\cdot\hat{i}$ and fits the time dependence to an appropriate model. More details on the technique can be found elsewhere.[13–15]

Such time-differential μSR measurements [in which $\mathbf{P}_\mu(t)$ rather than its integral is measured] fall into three geometric categories: longitudinal (LF), transverse (TF), and zero (ZF) field, depending on the direction of the applied magnetic field relative to the direction of the initial muon-spin polarization. The geometry for an LF (or a typical ZF) experiment is shown in Fig. 1. The muons enter from the left, pass through the thin muon (TM) detector and, via the aperture in the ''backward'' (B) positron counter, pass into the sample. The initial muon-spin polarization $\mathbf{P}_\mu(0)$ points backwards, and consequently, if the detection characteristics of the two symmetric counters are otherwise balanced, the B counter will initially detect more positrons on average than its ''forward'' (F) counterpart. One can measure the spin relaxation rate if appreciable relaxation occurs within the time window of observation—typically about $5\tau_\mu$. Often, $\mathbf{P}_\mu(t)$ simply decays exponentially (e.g., see Fig. 15), and the LF relaxation rate is exactly analogous to T_1^{-1} in NMR. In ZF, both T_1 processes and inhomogeneous static internal fields (for example, nuclear dipolar fields) contribute to the relaxation of $\mathbf{P}_\mu(t)$; whereas, in longitudinal fields exceeding the magnitude of any static internal fields, $\mathbf{P}_\mu(t)$ relaxes only

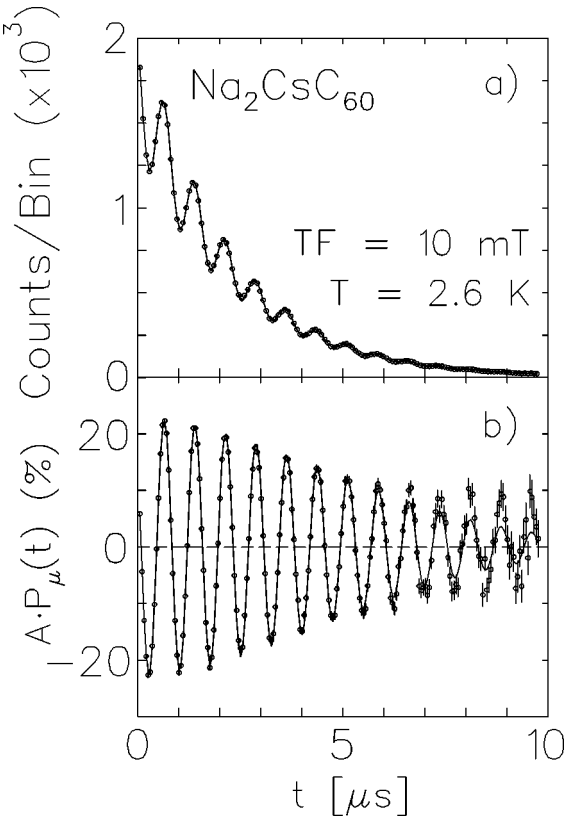

FIG. 2. (a) A histogram of time differences between muon implantation and decay, as detected in a single positron counter, in Na_2CsC_{60} in 10 mT transverse field. (b) The same data combined with another histogram to remove the muon lifetime. A small nonrelaxing signal, due to muons not stopping in the sample, is evident at late times. The relaxation is discussed in Sec. VI.

by T_1. ZF μSR is thus a very sensitive site-based probe of static magnetism. In the TF geometry, $\mathbf{P}_\mu(0)$ is perpendicular to $\mathbf{H}$, and $\mathbf{P}_\mu(t)$ exhibits oscillations at the Larmor frequency determined by the value of the magnetic field at the muon and the gyromagnetic ratio, $\gamma_\mu = 135.54$ MHz/T. The TF experiment is analogous to the free-induction decay of NMR with the TF relaxation rate being identified with T_2^{-1}. An example of the time histogram of a single counter in a TF experiment [following Eq. (2.1)] is given in Fig. 2(a).

The samples used in the measurements described here were made by intercalating alkali atoms into C_{60} at high temperatures. The details of this procedure can be found in, for example, Ref. 16. The samples were initially characterized by x-ray diffraction and magnetization. The grain size of the powders was $\sim 10^4$ Å, but the x-ray linewidths gave a crystalline coherence length, ξ_{XTL} of 500–1000 Å. From magnetization measurements in the superconducting state, the shielding fraction was typically 60%, and the Meissner fraction 10%. For the experiments described here, typically a few hundred milligrams of the powder was sealed under 1 atmosphere of 90% Ar/10% He in an aluminum vessel with a Kapton window which is thin enough to be easily penetrated by the muons.

A schematic diagram (approximately to scale) of the typical setup is shown in Fig. 3. The four side counters were used in the TF measurements, and the cup-shaped F counter and annular B counters were used in the LF and ZF measurements. The sample cell, F counter, and sample thermometers were mounted on the end of a lucite lightguide sample rod in the He space of a helium gas-flow cryostat. For the standard sample cell, a high-purity annular silver mask was placed immediately in front of the cell so that most of the muons that did not enter the sample cavity would stop in the silver and contribute only a benign temperature independent background. Between the beamline vacuum and the sample, the muons passed through four Kapton windows, the muon counter, a small air gap, a thin aluminized Mylar heat shield, and a small gap in cold helium gas. The total stopping density that these intervening obstacles presented to the muons was about 63 mg/cm^2. Precautions were taken to keep this density as small and constant as possible by preventing condensation on the outer cryostat window and limiting the pressure of the He gas at low temperature. At high fields, the helical positron paths have curvature on the scale of the detectors, and the effective solid angles of the counters consequently change. For example, the count rate in the B counters shown in the figure fall off significantly above about 2 T. Subsequent improvements to the B counters reduced this problem. The initial[17] data on $R_3^6C_{60}$ and some of the data presented here used only the F counter, while some of the data (e.g., see Fig. 15) used both F and B.

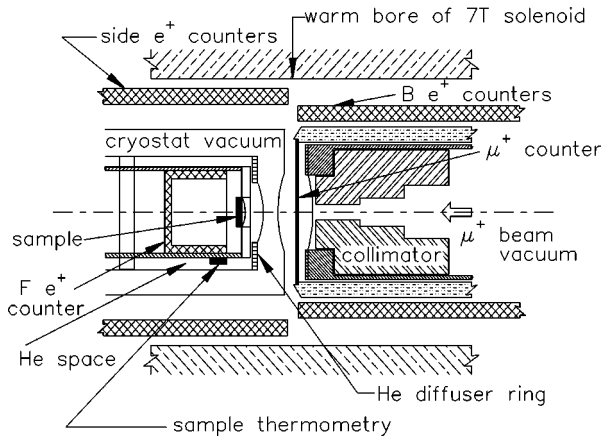

FIG. 3. Sketch of the apparatus. The superconducting solenoid bore is 15 cm in diameter and 61 cm in length. For the LF experiments the counters used were the cup-shaped F counter, directly behind the sample, and the cylindrical B counter surrounding the beampipe. For the TF experiments the side counters were used.

III. SPIN EXCHANGE RELAXATION OF MUONIUM

In this section, we include a brief description of muonium (the bound hydrogenic atom μ^+e^-) and its T_1 spin relaxation due to collisions with free electrons. A comparison with analogous nuclear-spin relaxation is also made.

The spin Hamiltonian for an isolated isotropic Mu is

$$H/h = \gamma_e \mathbf{S}_e \cdot \mathbf{B} + \gamma_\mu \mathbf{S}_\mu \cdot \mathbf{B} + A_\mu \mathbf{S}_e \cdot \mathbf{S}_\mu , \qquad (3.1)$$

where γ_i are the gyromagnetic ratios of the muon and electron, A_μ is the electron-muon hyperfine parameter (4463.302 MHz in vacuum), $\mathbf{S}_i$ are the spins and $\mathbf{B}$ is the applied magnetic induction. This Hamiltonian can be diagonalized analytically to give the field-dependent hyperfine energy levels which are plotted in a Breit-Rabi diagram, e.g., Fig. 4. The

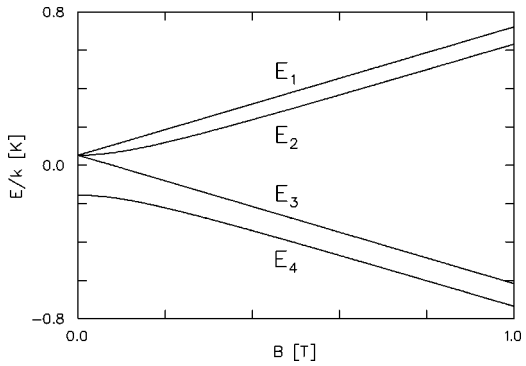

FIG. 4. Breit-Rabi diagram: The field dependence of the hyperfine energy levels (in Kelvin) of an isotropic muonium atom. The hyperfine coupling parameter here is the value for free Mu, $A = 4463.302$ MHz.

transition frequencies are conventionally[13] labeled $\nu_{ij}=(E_i - E_j)/h$, with E_i numbered according to Fig. 4. More detailed accounts of Mu (including anisotropic hyperfine interaction) can be found elsewhere.[13,18]

In metals, the predominant mechanism for T_1 relaxation of *nuclear*-spin polarization is via interaction with the conduction electrons within kT of the Fermi surface.[19,20] The interaction is usually modeled[20,21] by a direct hyperfine contact Hamiltonian:

$$H^i = A_n \mathbf{I}\cdot\mathbf{S}, \tag{3.2}$$

where the coupling A_n depends on the square modulus of the band electron wave function at the nucleus. The analogous coupling for a bare muon in conventional metals causes relaxation which is almost always too slow to observe on the muon time scale[22] (i.e., $T_1 \gg 10\ \mu$s) (see Sec. 3.2.4 of Cox[14]). The actual coupling mechanism relevant for NMR T_1 in A_3C_{60} has, in addition to Eq. (3.2), an important anisotropic contribution originating from the full electron-nucleus magnetic dipolar interaction, as discussed in detail elsewhere.[23,24] For endohedral muonium in A_3C_{60}, we are in the unusual situation of having a tightly bound paramagnetic muonium center in a metallic environment. The interaction between a paramagnetic center and the conduction electrons is more complicated than Eq. (3.2) because of the extra degrees of freedom of the bound electron. Nevertheless, we can model the interaction in a similar way. The spin-independent Coulomb interaction between the conduction electrons and the local muonium electron in conjunction with the Pauli principle yields the simple spin-exchange Hamiltonian:

$$H^i = J(r)\mathbf{S}_e\cdot\mathbf{S}_e^{\mathrm{Mu}}, \tag{3.3}$$

where r is the separation of the scattering electron and the Mu atom, and $J(r)$ is a short-range scattering potential.[25] The effect of this interaction is to randomly flip the muonium electron spin (Fig. 5), consequently producing a random modulation of the hyperfine field at the muon and causing the muon's spin to relax.

The theory of such spin relaxation has been worked out in several contexts using various methods.[26] For the case of isotropic Mu hyperfine coupling A_μ, the behavior of the LF (T_1) muon-spin-relaxation rate due to spin exchange is divided into two regimes by a crossover when the rate of spin-exchange events (ν_{SE}) equals the ''2–4'' muonium hyperfine frequency (ν_{24}), which at high fields ($B \gg A_\mu/\gamma_e$) is approximately the electron Zeeman frequency. In the fast region ($\nu_{\mathrm{SE}} \gg \nu_{24}$), the relaxation rate is approximately field independent, and in the slow regime the relaxation rate is governed by

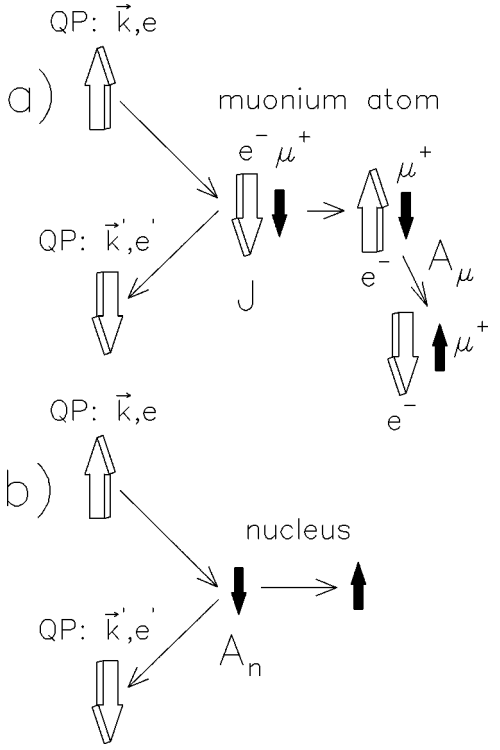

FIG. 5. In each case a quasiparticle (QP) at the Fermi surface with initial momentum **k** and energy e scatters magnetically from the local moment. (a) Spin exchange of a muonium atom (with subsequent evolution due to the muon-electron hyperfine interaction A_μ) vs (b) electron-nuclear spin flip. In the spin exchange with the paramagnetic muonium, the electron Zeeman energies cancel, whereas in the latter, the nuclear and electron Zeeman energies do not.

$$T_1^{-1} \approx \frac{A_\mu^2 \nu_{\mathrm{SE}}}{2\{A_\mu^2 + [(\gamma_e + \gamma_\mu)B]^2\}}. \tag{3.4}$$

The origin of this relaxation lies in the field dependence of the spin eigenstates of Mu as explained elsewhere.[27]

It has also been shown[27] that the relaxation rate in the case where the muonium hyperfine interaction is anisotropic can be dramatically different. There is a peak in $T_1^{-1}(B)$ at a field determined by the principal values of the hyperfine parameter. While this peak has only been observed in doped crystalline semiconductors, it is expected to survive, in perhaps a very broadened form, an orientational powder average. From the high symmetry of the site at the center of the C_{60} cage, we expect Mu@C_{60} have an essentially isotropic hyperfine interaction, but *a priori* one might expect that Mu inside the cage could bond to a single carbon, forming a highly anisotropic endohedral radical. Calculations[28] suggest that such a state is not stable. In pure and insulating alkali-doped C_{60} phases,[29,30] this conclusion is confirmed by observation of very narrow coherent spin precession lines from

$Mu@C_{60}$. In contrast, when muonium bonds exohedrally to form a $C_{60}Mu$ radical a much broader line at low temperature is observed due to the anisotropic hyperfine interaction (see Fig. 8). Simulations for muonium with a large nearly isotropic hyperfine interaction, indicate that deviations from Eq. (3.4) will occur only at extremely high fields where the *muon* Zeeman energy is comparable to the hyperfine interaction.

In analysis of the temperature dependence of the relaxation rate, it is of interest to consider the degree of inelasticity of the direct and spin-exchange scattering processes. In the case of the direct interaction Eq. (3.2), the nuclear-spin and conduction-electron spin flip-flop (Fig. 5), requiring an energy $\alpha_m=|(\mu_B-\mu_{\rm nuc})B|$; whereas, in the muonium spin-exchange event Eq. (3.3), the electron Zeeman energies balance and the energy required is

$$\alpha_m=A_\mu/2, \tag{3.5}$$

independent of magnetic field. For the case of vacuum muonium α_m corresponds to a temperature of about 0.1 K compared to an $\alpha_m(B=10\ \text{T})$ of 13.4 K for Korringa relaxation of nuclear spins.

IV. SPIN RELAXATION IN SUPERCONDUCTORS

A. General

The effective interactions Eqs. (3.2),(3.3) between the conduction electrons of a metal and a nuclear or muonium electron spin may be treated as first-order scattering problems.[20] According to Fermi's golden rule, the rate of transitions between spin states is determined by

$$W_{ab}=\frac{2\pi}{\hbar}\sum_{\mathbf{k},\sigma,\mathbf{k}',\sigma'}|\langle a\mathbf{k}\sigma|H^i|b\mathbf{k}'\sigma'\rangle|^2 \times\delta(E_{\mathbf{k}}-E'_{\mathbf{k}}+\alpha_m)f_{\mathbf{k},\sigma}[1-f_{\mathbf{k}',\sigma'}], \tag{4.1}$$

where $\mathbf{k}$ and σ label the conduction-electron momentum and spin states; $E_{\mathbf{k}}$ is the corresponding kinetic energy and $f_{\mathbf{k},\sigma}$ the occupation probability; a and b label the nuclear or muonium spin states; and $\alpha_m(\sigma_i)$ is the change in magnetic energy. One may convert the sum in Eq. (4.1) to an integral over energy in the usual way, using the (normal state) electronic density of states (DOS), $g_N(E)$, where E is measured relative to E_F. Using $g_N(E)\approx g_N(0)$ within kT of E_F to simplify the integral, one obtains the Korringa law:

$$R_N\equiv(T_1^{-1})_N\propto g_N^2(0)kT. \tag{4.2}$$

In the superconducting state, the expression for the nuclear transition probability Eq. (4.1) is formally the same, but the scattering is accomplished by the bogolons (quasiparticle excitations of the superconducting state), which differ in two important respects from conduction electrons of the normal state: (i) there are phase correlations between states of opposite momentum and spin which necessitate combination of pairs of matrix elements *before* squaring (see, e.g., Sec. 3.9 of Tinkham[31]) and give rise to the ''coherence factors;'' and (ii) the excitation spectrum near E_F is strongly modified: the DOS is gapped and the gap is flanked on either side by peaks. The BCS theory[32] predicted that these peaks would have the singular form [see Fig. 6(a)]:

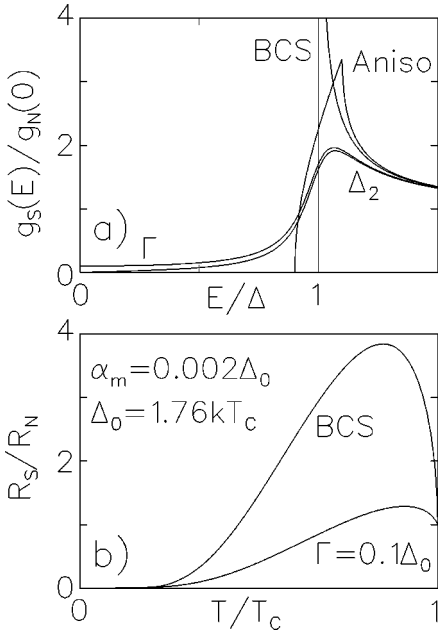

FIG. 6. (a) Models of the superconducting DOS: BCS is g_S of Eq. (4.3), Aniso is g_A [Eq. (4.6)] with a gate function distribution $P(a)$ of width 0.1Δ, Γ is g_D [Eq. (4.7)] with $\Gamma=0.1\Delta$, and Δ_2 is g_{SC} [Eq. (4.8)] with $\Delta_2=0.1\Delta$. (b) The value of the Hebel-Slichter integral for the BCS and lifetime [Eq. (4.7)] broadened g_S(E). The magnetic inelasticity parameter (α_m) is appropriate for $Mu@C_{60}$ in Rb_3C_{60}. The BCS temperature dependence $\Delta(T)$ was used.

$$g_S(E)=g_N(E)\,\mathrm{Re}\left\{\frac{|E|}{\sqrt{E^2-\Delta^2}}\right\}, \tag{4.3}$$

where Re is the real part, E is the energy measured from E_F, and $\Delta(T)$ is the order parameter, which for the moment we consider to be real, isotropic and homogeneous. Applying these modifications, we get the following integral for the T_1 relaxation rate in the superconducting state (normalized to the rate in the normal state)[33]

$$\frac{R_S}{R_N}=2\beta\int_0^\infty \mathrm{Re}\left\{\sqrt{\frac{(EE'+\Delta^2)}{(E^2-\Delta^2)}}\right\} \times\mathrm{Re}\left\{\sqrt{\frac{(EE'+\Delta^2)}{(E'^2-\Delta^2)}}\right\}f(E)[1-f(E')]dE, \tag{4.4}$$

where $\beta=(kT)^{-1}$, f is the Fermi-Dirac distribution function, and $E'-E=\alpha_m$. Neglecting any spin polarization of the quasiparticles, the exothermic and endothermic scattering events will be equally probable, and we take the ratio R_S/R_N to be the simple average of the integrals Eq. (4.4) with α_m both positive and negative. If the inelasticity of the collisions is neglected ($\alpha_m=0$), the two singularities in the integrand coalesce, and the integral becomes logarithmically divergent; however, the singularity is not a practical problem because α_m is finite, and, more importantly, the peak in the DOS is broadened from the BCS result Eq. (4.3), as will be discussed in detail in Sec. IV C. As a function of decreasing temperature, Eq. (4.4) exhibits a peak just below T_c, due to the peaked DOS factors, and at lower temperatures, falls off

exponentially. For $\alpha_m \approx 0.002\Delta(0)$ (appropriate to the case of Mu in Rb_3C_{60}, if it is a BCS superconductor), and assuming the BCS temperature dependence $\Delta(T)$, the maximum of R_S/R_N is about 4 [see Fig. 6(b)].

B. Low-temperature behavior

Typically, the low-temperature behavior of Eq. (4.4) is approximated by an Arrhenius law,

$$R_S/R_N \sim \exp(-\Delta_0/kT), \tag{4.5}$$

while this certainly accounts for the majority of the low-T dependence, it is not the complete dependence. Perfect Arrhenius behavior is only rigorously found if the integrand of Eq. (4.4) is gapped but otherwise featureless in energy. The strongest energy dependence one might expect in the integrand (for a gapped density of states) is that of BCS. Allowing for finite α_m, the singular behavior of the square of the BCS density of states is avoided, and the integral can be expanded at low T in terms of modified Bessel functions, giving a temperature-dependent prefactor to the Arrhenius dependence of $T^{-1/2}$. This is analogous to the temperature dependence of the penetration depth.[31,34,35] $T^{-1/2}$ is a weak function of temperature compared to Eq. (4.5), but it does lead to a significant bias in the energy gap extracted using Eq. (4.5). For example, if one fits Eq. (4.5) to data that varies as $T^{-1/2}\exp(-1.76T_c/T)$, over a range of reduced temperature $t=T/T_c$ of 0.25–0.5 (typical for many NMR studies), one finds $\Delta_0 = 1.56kT_c$, and the Arrhenius plot does not deviate noticeably from linear. While the specific $T^{-1/2}$ dependence is highly idealized, this example illustrates the dangers of using a simple model such as Eq. (4.5) especially over a restricted range in temperature. The low-temperature behavior in cases less ideal than Eq. (4.3) will be determined by balancing the contributions of both the peak in $g(E)$ at Δ (if it is present), and any finite $g(E)$ within the ''gap,'' with the latter always dominating at the lowest temperature because of the exponential weighting of the Fermi factor. We will consider more realistic models for $g(E)$ in the next section.

C. Extensions

The temperature dependence of Eq. (4.4) discussed above can be modified through several mechanisms which we will consider in turn: anisotropy of Δ, finite lifetime of quasiparticle excitations, and magnetic effects. The consequences of anisotropy on the ratio R_S/R_N are found by including an angular integral in Eq. (4.4), and they can be most easily explained by a comparison between the angular average DOS, $g_A(E)$, and $g_S(E)$ of Eq. (4.3):

$$g_A(E) = g_N(E)\mathrm{Re}\left\{ \int_{a1}^{a2} \frac{E}{\sqrt{E^2-\Delta_G^2(1+a^2)}} P(a)\,da \right\}, \tag{4.6}$$

where $P(a)$ is the distribution of the anisotropy a of the gap around the Fermi surface. Even a small anisotropy, such as that for aluminum,[33] transforms the BCS singularity in $g_S(E)$ into a mild van Hove singularity at some average Δ_P, and g_A is still perfectly gapped with $g_A(E)=0$ for $|E| \leqslant \Delta_G$ [see Fig. 6(a)]. The effect of anisotropy is thus to reduce the size of the coherence peak in R_S/R_N and to modify the Arrhenius slope relative to the isotropic case. Extreme anisotropy, such as that for nonzero angular momentum pairing states, is similar except that g_A is no longer gapped as there are nodes in Δ. For example, for a d-wave order parameter,[36] $g_A(E) \propto E$ as $E \to 0$. Although g_A is still peaked in this situation, the coherence peak in R_S/R_N may be completely eliminated,[37] and the exponential temperature dependence is replaced by a power law $R_S/R_N \propto T^p$, where $p=2$ for d wave, and other values of p are obtained[38] for different nodal structures of Δ. This kind of behavior has been observed[39,40] in $YBa_2Cu_3O_{6.95}$, for which there is strong evidence of a d-wave Δ. A p-wave Δ may be the source of similar temperature dependence in some Heavy Fermion superconductors,[41,42] while it may be related to near $1d$ behavior in some organic superconductors.[43]

Finite lifetime (τ) of the quasiparticle excitations of a superconductor due, for example, to electron-phonon, electron-electron or impurity scattering can also modify R_S/R_N. This possibility was suggested by Hebel and Slichter in their original work[21] to explain the small size of the coherence peak they observed in Al. They calculated a DOS which was a version of Eq. (4.3) smeared by convolution with a gate function of width τ^{-1}. A detailed analysis of the temperature dependence of R_S/R_N resulting from this approximation is given by Hebel.[44] A different Ansatz for the DOS was used by Dynes *et al.*[45] to describe tunneling measurements:

$$g_D(E) = g_N(E)\mathrm{Re}\left\{ \frac{E+i\Gamma}{\sqrt{(E+i\Gamma)^2-\Delta^2}} \right\}, \tag{4.7}$$

where $\Gamma \sim \tau^{-1}$. However, Allen and Rainer[46] point out that for a lifetime due to *electron-phonon* scattering, one must resort to the Eliashberg theory of strongly coupled superconductors[47,48] in which the order parameter becomes complex, and the DOS is[49]

$$g_{SC}(E) = g_N(E)\mathrm{Re}\left\{ \frac{E}{\sqrt{E^2-(\Delta_1+i\Delta_2)^2}} \right\}, \tag{4.8}$$

where[50] $\Delta_2 = \mathrm{Im}\ \Delta \sim \tau^{-1}$ (Im is the imaginary part), and $\Delta = \Delta(E,T)$ is determined by the Eliashberg theory and the coupling constant-phonon spectrum product $\alpha^2F(E)$ for the particular material. Fibich[51] treated the problem of calculating R_S/R_N using Eq. (4.8) by neglecting the energy dependence of Δ, and simply using Δ evaluated at the energy which is most important for the integral Eq. (4.4), i.e., $\Delta[E=\Delta_1(T),T]$. The temperature dependence for the imaginary part $\Delta_2(T)$ due to phonon scattering[51,52] and scattering from other quasiparticles[50,53] has been calculated in the low temperature limit. For the temperature dependence of the real part $\Delta_1(T)$ (and for the parameter Δ in either of the preceding models) it is reasonable[47] to assume that the temperature dependence of the real part of the order parameter is approximately that of the BCS Δ. Recently, it has become feasible[54,46] to calculate R_S/R_N using the full strong-coupling $\Delta(E,T)$, thus avoiding these approximations. As input to such a calculation, one would ideally first obtain a reasonable form for $\alpha^2F(E)$. However, according to Akis,[54] the details of $\alpha^2F(E)$ are not important, and the most sig-

nificant information in determining $R_S/R_N(T)$ is summarized in the ratio $T_c/E_{\ln}$, where $E_{\ln}$ is the logarithmic moment of $\alpha^2F(E)$,

$$E_{\ln}=\exp\left[\frac{2}{\lambda}\int_0^\infty \alpha^2F(E)\frac{\ln(E)}{E}dE\right], \tag{4.9}$$

where λ is the mass enhancement parameter, $2\int_0^\infty[\alpha^2F(E)/E]dE$. Note that the effect of impurities in the Eliashberg theory has recently been revisited.[55] These authors find that ''vertex corrections'' from impurity scattering can *increase* the size of the coherence peak as the mean free path is reduced.

Magnetism may also influence $R_S/R_N(T)$, for instance, in the classical example[56] of gaplessness in a superconductor due to the presence of magnetic impurities, the coherence peak can be reduced or eliminated and the exponential falloff altered significantly.[57,58] Superconductors that are intrinsically magnetic exhibit similar strong deviations.[41,59] In regard to high-T_c superconductors, antiferromagnetic correlations between quasiparticles have also been shown[37,54] to damp the coherence peak. However, it should be noted that no anomalous behavior connected with magnetism has been reported yet in A_3C_{60}. Recently,[60] the closely related $NH_3K_3C_{60}$ material which is superconducting under high pressure has been found to exhibit a metal-insulator transition to a magnetic state[61] at about 40 K. The small bandwidth and large Coulomb interactions between electrons also cause important correlation effects, for example the magnetism in orthorhombic AC_{60}. The proximity to a similar magnetic phase may be enhanced by the analogous polymerization[62] of the C_{60} anions in the $Pa\bar{3}$ materials.

D. Influence of the vortex state

Measurements of T_1 in type-II superconductors ($\lambda > \sqrt{2}\xi$), including those presented below, are typically done with the applied field above the lower critical field, H_{c1}, i.e., in the vortex state. One must therefore consider the modifications to the zero-field situation discussed above, due to the presence of the field. The magnetic field interacts with the electronic system in two ways: (i) via the Lorentz force embodied in the canonical momentum $\mathbf{p}+q\mathbf{A}$ and (ii) via the Zeeman interaction of the electronic spins $\boldsymbol{\mu}\cdot\mathbf{B}$, consequently modifying the quasiparticle excitation spectrum and hence the temperature dependence of R_S/R_N relative to Eq. (4.4).

The Lorentz force, together with the magnetic-field energy, yields the vortex structure of the mixed state wherein the field and the order parameter are *inhomogeneous*, for example, the Abrikosov flux lattice (see the review[63]) or more disordered phases.[64] Near H_{c2}, where the order parameter is small, the effect of the inhomogeneity $\Delta(\mathbf{r})$ has been treated theoretically in the dirty[65] and clean[66] limits and, subsequently, for arbitrary[67] mean free path l. In the dirty limit the effect of the DOS (Ref. 65) is in close analogy with the Abrikosov-Gor'kov theory of gapless superconductivity[68,69] in the presence of magnetic impurities,

$$g(E,\mathbf{r})\approx g_N(E)\left\{1+\frac{|\Delta(\mathbf{r})|^2}{2}\frac{E^2-\eta^2}{(E^2+\eta^2)^2}\right\}, \tag{4.10}$$

where η is the pair-breaking perturbation parameter,[68,65] $\eta \propto \tau B$, where τ is the collision time. The DOS exhibits no gap. In the clean limit[66] the (angle-resolved) DOS is highly anisotropic with singular BCS [Eq. (4.3)] behavior along the magnetic field and gapless behavior perpendicular to the field. The latter property has been confirmed and exploited in measurements of de Haas-van Alphen oscillations in the mixed state at high fields.[70] The effect of finite mean free path in this case is to wash out the anisotropy (and with it the BCS singularity) and to make the density of states a rigorously local property.[65]

Away from H_{c2}, the expansions assuming small Δ are not applicable. The more general theories are very complex, but some approximate results have been obtained. There are two main approaches used to calculate properties of the vortex state in the regime $H_{c1}\ll H\ll H_{c2}$: the Green's-function approach of Gor'kov[71] and the effective Hamiltonian approach of Bogoliubov and deGennes.[65] Using the second approach, the presence of bound, nearly gapless excitations in the vortex cores was predicted.[72] Far from the vortex cores, the excitation spectrum is modified only by the ''Doppler shift'' of the quasiparticle energies due to the circulating supercurrents. Neglecting the core states, Cyrot[73] calculated an explicitly field-dependent DOS. These calculations show that the peaks of the zero-field DOS are broadened significantly as the vortex spacing decreases below about 10ξ. Motivated by scanning tunneling microscopy (STM) measurements of the detailed spatial structure of the vortex state, this method has been revisited recently, e.g., see Refs. 74,75. In contrast to the local nature of the dirty limit, where the core contributions can be modeled simply as normal electrons, in the clean limit, the interplay between the core states and the surrounding superconductor may be very important.[75] The Green's-function approach has been employed generally using a linearized version of Gor'kov's equations. For the dirty limit, the field-dependent local and spatially averaged DOS have been calculated numerically.[76] The spatially averaged DOS peaks in this calculation also exhibit field-dependent broadening. Clean-limit calculations have also been performed.[77] Recent use of this technique[78,79] has concentrated on the structure of the vortex core.

It has long been recognized[80] that the Zeeman interaction acts to break the Cooper pairs of a conventional superconductor because it acts in the opposite sense on each member of the pair. The magnetic field at which the Zeeman interaction will destroy superconductivity can be approximated by equating the gain in energy in going to the (spin-polarized) normal state with the condensation energy of the superconductor, thus defining[81] the Pauli limiting field B_P:

$$B_P(t)=\frac{B_c(t)}{\sqrt{(1+\chi_N)^2-[1+\chi_S(t)]^2}}, \tag{4.11}$$

where $B_c(t)$ is the thermodynamic critical field and χ_i is the spin susceptibility in each of the phases. The modification of the upper critical field H_{c2} due to these considerations has been calculated,[82,81] and its effect on the spectrum of excitations has been predicted to be negligible[68] unless there is some mechanism for mixing quasiparticle states of opposite spin, e.g., spin-orbit scattering. In the case of strong spin-orbit scattering, the quasiparticle spectrum is again of the

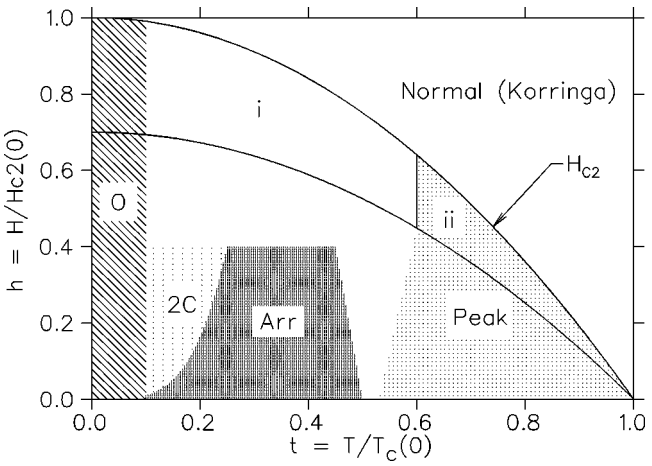

FIG. 7. A generic phase diagram for the behavior of $(T_1T)^{-1}$ in a conventional type-II superconductor. The regions are *Peak*, where the Hebel-Slichter coherence peak is found; *Arr*, where approximately activated behavior occurs, $2C$, where two component relaxation from the inhomogeneity of the vortex state is expected to be observed; O, where other processes may come to dominate the electronic relaxation rate (e.g., magnetic impurities). Further details are given in the text.

form Eq. (4.10) with the pair-breaking parameter $\eta \propto \tau_{so}B^2$, where τ_{so} is the time between spin-orbit scattering events.[68]

Despite these complications in the vortex state, many of the general features of the zero-field (Meissner) state behavior of R_S/R_N as discussed in Sec. IV A are observed experimentally. Figure 7 shows the phase diagram of the vortex state, for an extreme (H_{c1} coincides with the horizontal axis on this scale) type-II superconductor showing regimes of different behavior for T_1 in the most conventional case. To the lower right is the region of the Hebel-Slichter coherence peak. To the left is the ''Arrhenius region'' where the relaxation rate falls exponentially. Above about $0.7H_{c2}$, the theories based on the gaplessness due to a small inhomogeneous order parameter $\Delta(\mathbf{r})$ are applicable. In particular $R_S/R_N(T,l\rightarrow 0)$ has been calculated[83] with the result, that the peak is reduced but still present in region (ii), and completely eliminated in region (i). The high-field damping and elimination of the coherence peak predicted by this theory has been clearly verified experimentally[84] in the $A15$ superconductor V_3Sn. The calculation of $R_S/R_N(T,l)$ can be found elsewhere.[85]

Departures from the exponential falloff of the relaxation rate with temperature are typically seen at low temperature (region 2C). In this region, the much more weakly temperature dependent relaxation from the electronic excitations in the vortex cores can be significant.[86] One can model the relaxation of (muon or nuclear) spin polarization in such an inhomogeneous case using a local relaxation rate. The average relaxation function is

$$P_z(t)=\int_0^\infty dR\, e^{-Rt}P(R), \tag{4.12}$$

where the inhomogeneous T_1 rate $R[B(\mathbf{r}),\Delta(\mathbf{r}),T]$ is distributed as $P(R)$, and z indicates LF (T_1) relaxation. For $B \ll B_{c2}$, the vortices may be treated (in the dirty limit) approximately[72] as cylinders of normal-state material of radius ξ. The distribution $P(R)$ in this approximation is bimodal with peaks at R_N and R_S. The relaxation $P_Z(t)$ will not be single exponential, but the average relaxation rate is[87]

$$\langle R_S/R_N\rangle = f_N+(1-f_N)R_S/R_N, \tag{4.13}$$

where, for $(B \ll B_{c2})$, $f_N \sim \xi^2(B/\Phi_0)$, i.e., the weight in the distribution $P(R)$ at R_N scales linearly with field (Φ_0 is the magnetic flux quantum). This linear field dependence allows the deviation from exponential temperature dependence of the relaxation rate due to the vortex cores to be distinguished from the other mechanisms, such as impurity scattering, (region O) which at low temperature, and especially in low field, may dominate the electronic relaxation. From the field dependence, one can thus use this model to extract a rough estimate[88,87] of ξ deep in the superconducting state. Such estimates could be refined by including a more sophisticated local DOS (Refs. 78 and 74) in the model for $P(R)$, but dynamic effects might also require consideration. Motion of the vortices on the time scale T_1 would smear the distribution $P(R)$, effacing the bimodal structure of the static vortex state; however, vortex dynamics usually occurs on time scales much shorter than a typical T_1,[89] though exceptions have been proposed.[90] Another type of dynamics that has been considered in this context is that of spin diffusion of the nuclear magnetization to the quickly relaxing regions of the cores which effectively allows the relaxation to ''leak'' out of the vortex cores into the surrounding superfluid. This mechanism, though, may be thermodynamically quenched in the inhomogeneous vortex state.[91] Furthermore, such a mechanism is not important in the experiments described here because we are always dealing with a single muon in the sample at any time, and $Mu@C_{60}$ is static (at least on the length scale of the vortex lattice and on the time scale of the muon).

Deviations from the behavior summarized in Fig. 7 are expected and observed in many cases: Reduction of the peak region [towards $(t,h)=(1,0)$] may be the result of any of the mechanisms discussed in the previous section. More detailed reviews of NMR in type-II superconductors can be found elsewhere.[33,92,93]

V. μ^+ SITES IN A_3C_{60}

When muons stop in typical metals, they take up one or a few well-defined crystallographic sites, usually interstitial. In the vast majority of cases there is no local electronic moment on the muon, and the muon is said to be in a local diamagnetic state. In insulators and semiconductors, μ^+ often captures an electron to form paramagnetic muonium which also occupies a specific interstitial site; however, the paramagnetic states almost never occur in metallic environments. Screening of the electrostatic potential by conduction electrons eliminates any local electronic level with a single unpaired electron. Although the details of the particular sites adopted by the muon are not critical to the analysis we report in the following sections, a brief discussion is included here for completeness.

In C_{60}-based solids, the available interstitial voids are much larger than in conventional metals, and there are many potential sites for the muon, though some are occupied by alkali ions in the alkali fullerides, i.e., the octahedral (O) and

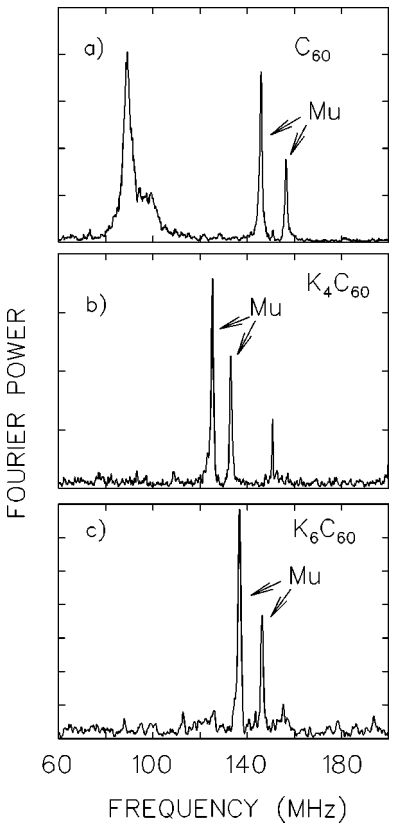

FIG. 8. The precession signals of endohedral muonium in (a) C_{60} at 10.7 mT, (b) K_4C_{60} at 9.6 mT, and (c) K_6C_{60} at 10.0 mT [from Kiefl (Ref. 29)]. The broad line in C_{60} is due to the C_{60}Mu molecular radical, and the narrow line at 150 MHz in the K_4C_{60} spectrum is an instrumental effect. The frequencies and their field dependences correspond to vacuumlike Mu with $A_\mu = 4341(24)$, 4342(66), and 4230(63) MHz, respectively.

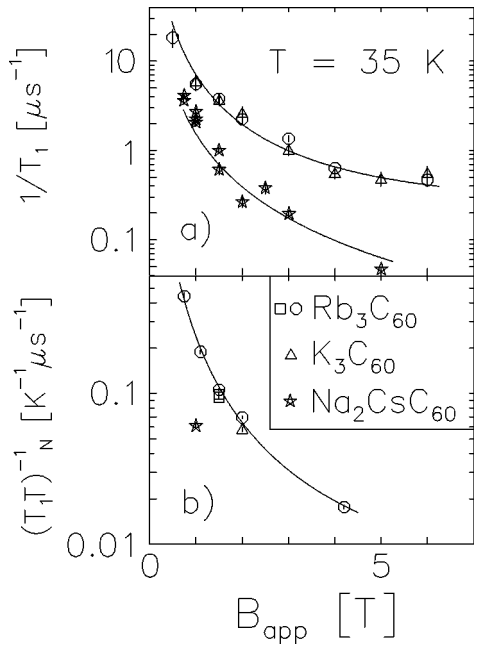

FIG. 9. (a) The field dependence of the LF relaxation rates at 35 K. The fits to the spin-exchange model in the slow limit are discussed in the text. (b) The field dependence of the normal-state value of $(T_1T)^{-1}$ fit to a similar model.

tetrahedral (T) interstitial sites. In pure C_{60}, $\sim$80% of the implanted muons form an exohedrally bonded muonium radical (C_{60}Mu) which has been studied extensively.[30,94,28] In the ionic insulating fullerides K_4 and K_6,[29] and the conductors Rb_1 (Ref. 95) and Rb_3,[17] a similar fraction of the muons exhibit diamagnetic behavior. Thus in both metallic and insulating environments, the exohedral C_{60}Mu radical does not survive the charging of the C_{60}. The diamagnetic muons in fcc A_3C_{60} are certainly interstitial in the lattice of C_{60}^{-3} ions, but their precise position(s) are not known. One possibility is that as the Fermi level rises upon alkali-metal doping, the interstitial muons become negatively charged and form a complex with the alkali metal ion analogous to an alkali-hydride molecule.

In both pure C_{60} and the insulating alkali fullerides, a small fraction of implanted muons ($\sim$10–20%) form a muonium atom characterized by a large isotropic hyperfine parameter which has been interpreted[96,30,29] to be trapped endohedral muonium [Mu@C_{60} pictured in Fig. 11(a)]. Figure 8 shows the clear signature for this state, i.e., TF precession at frequencies determined by the hyperfine levels of Fig. 4. In the metallic systems, however, these precession signals are expected to be unobservable due to broadening either via the Korringa mechanism or by inhomogeneous broadening in the vortex state of the superconductor or in the low-temperature magnetic phases of the *A* metals. One possibility for observation of the oscillation, however, is at the lowest temperature in zero field in the Meissner state of an A_3 superconductor, where a high-frequency ''heartbeat'' oscillation ($\approx$4.4 GHz) might be observed because the Korringa and inhomogeneity broadening mechanisms will be negligible. Such high-frequency measurements are technically quite difficult[97] and have not yet been attempted.

Coherent precession signals from Mu@C_{60} are not expected in a conductor due to rapid spin exchange with conduction electrons. However, the presence of Mu@C_{60} can be confirmed in LF experiments. Specifically, provided the T_1 relaxation of the μ^+ in the Mu@C_{60} atom is in the muon time range, the relaxation rate will have the characteristic magnetic-field dependence of Eq. (3.4). We have observed this relaxation in the A_3 superconductors and measured its field dependence at $T = 35$ K (well into the normal state). The relaxation is single exponential, and the rates as a function of field are plotted in Fig. 9(a). The fits shown are to Eq. (3.4) with a small additional field-independent rate, R_0. Because the parameters A_μ and ν_{SE} are correlated, they could not be determined independently, and we fixed $A_\mu = 4340$ MHz from the precession measurements in the insulators (Fig. 8). This value is also consistent with LF measurements of A_μ in Rb_3 discussed below. The resulting parameters are given in Table I along with the ratios

$$\rho^x_{35\,\mathrm{K}} = \sqrt{\frac{\nu^x_{\mathrm{SE}}(35\ \mathrm{K})}{\nu^{Rb3}_{\mathrm{SE}}(35\ \mathrm{K})}}. \tag{5.1}$$

From the Korringa Law, Eq. (4.2), this ratio is a measure of the ratio of the density of states at the Fermi surface $g_N(0)$ relative to its value in Rb_3. Additionally, it is reasonable to assume A_μ is not very temperature dependent at low temperature, as is evidenced by Korringa temperature depen-

TABLE I. Parameters of the fits of $T_1^{-1}(B)$ at 35 K to Eq. (3.4) with $A_\mu = 4340$ MHz as well as the ratios defined (relative to Rb_3) in the text.

	ν_{SE} (35 K) (MHz)	R_0 (μs^{-1})	$\rho^x_{35\,K}$	ρ^x
Rb_3C_{60}	587(47)	0.217(70)	1	1
K_3C_{60}	572(63)	0.215(50)	0.987(94)	0.950(31)
Na_2CsC_{60}	132(4)	0.0000(2)	0.474(25)	0.506(20)

dence of the relaxation rate in the normal state which is entirely the temperature dependence of ν_{SE}. Hence we can also fit the more accurately determined average value of $(T_1T)^{-1}$ in the normal state to Eq. (3.4). These average values over several temperatures above T_c are shown in Fig. 9(b). Fitting the Rb_3 results to Eq. (3.4) with $A_\mu = 4340$ MHz yields $\nu_{SE}/T = 20.2(4)$ MHz/K with $R_0/T = 4.4(7)\times 10^{-3}$ μs^{-1}/K. Using this fit and the points for K_3 and Na_2Cs, we calculate the ratios,

$$\rho^x = \sqrt{\frac{(T_1T)_N^{Rb3}}{(T_1T)_N^x}}, \tag{5.2}$$

which are also given in Table I.

The low values of ν_{SE} (relative to A_μ) confirm that the slow spin-exchange limit form Eq. (3.4) is justified at this temperature and below (for all fields). In fact, ν_{SE} is remarkably slow compared to spin-exchange rates of Mu in semiconductors such as Si. In that case the spin-exchange rate is usually[18] modeled as

$$\nu_{SE} = \sigma n(T) v(T), \tag{5.3}$$

where one has extracted the majority of the temperature dependence of the Golden rule expression [Eq. (4.1)] into the carrier concentration, n, and the mean thermal velocity v, leaving the nearly temperature independent sum over matrix elements in the appropriately defined cross section σ. For interstitial Mu in Si, the observed ν_{SE} implies that σ is of the order of a typical atomic cross section (10^{-15} cm^2). In the metallic case the situation is different since Fermi blocking prevents all but the electrons within kT of the Fermi surface from participating in the spin-exchange collisions. Thus $v \approx v_F$, the Fermi velocity and is nearly T independent, and $n \approx n_0 kT/E_F$. Using values[5] for Rb_3 ($v_F \approx 10^{-7}$ cm/s, $E_F \approx 0.5$ eV, $n_0 \approx 4\times 10^{21}$ cm^{-3}), σ for Mu@C_{60} is 10^{-18}–10^{-19} cm^2 at 35 K. The small size of σ is attributed to the combination of two factors. First, the conduction-band states are made up of C_{60} molecular orbitals in which the electrons are confined near the hollow carbon cage. The spatial distribution of the conduction electrons is thus quite inhomogeneous on the scale of the unit cell, and Mu@C_{60} is located in a site of low conduction-electron density. Second, possibly for geometric reasons, there is very little hybridization of Mu@C_{60} with the surrounding C_{60} orbitals. The sp^2 carbon orbitals are distorted by curvature of the C_{60}, so that the inner lobes are smaller than the outer ones. Consequently, the tendency for bonding is significantly greater on the outer surface of the molecule.[28] The evidence for this is the large vacuumlike isotropic Mu hyperfine interaction. This is also consistent with the apparently very small ^{13}C-Mu nuclear hyperfine interaction[29] in pure C_{60}. In contrast, in semiconductors, the hyperfine parameters of muonium are much lower than the vacuum value.[18] We thus conclude that for Mu@C_{60} the spin-exchange interaction [J in Eq. (3.3)] in A_3C_{60} is small and the perturbation approach Eq. (4.1) is valid.

Comparison of the dependence of the DOS at the Fermi surface $g_N(0)$ on lattice constant a with the dependence of $T_c(a)$ elucidates the exponent of the McMillan equation; furthermore, there is considerable interest in the role of orientational disorder in determining electronic properties such as $g_N(0)$.[98,99] For comparison, similar ratios from NMR (Refs. 100,101,24, and 102) yield $\rho^x > 0.75$ for both $x = K_3$ and Na_2Cs. The low value of our ratios for Na_2Cs *may* indicate that the proportionality constants (hyperfine couplings) between ν_{SE} [or $(T_1T)^{-1}$] and $g_N^2(0)$ may vary with structure. This is not unreasonable, since the couplings depend on the detailed structure of the electronic orbitals constituting the conduction band, such as the degree of sp hybridization. It is known that the C-C bond lengths of C_{60}^{-3} in cubic Na_2Cs differ slightly[7] from those of the neutral C_{60}, but similar measurements on the orientationally disordered systems have not been reported. The exchange coupling for Mu@C_{60} [J in Eq. (3.3)] may be more sensitive to such differences than those of ^{13}C NMR because they are determined by the tails of the carbon orbitals protruding into the ball; whereas, the NMR constants are determined by the behavior of the orbitals at or near the ^{13}C nucleus. While the electron-phonon enhancement of g_N (which may differ between the $Pa\bar{3}$ and $Fm\bar{3}m$ structures) does not[103] affect T_1, electron-electron interactions can,[23] via for example, Stoner enhancement of $g_N(0)$. If there are short-wavelength electronic correlations, it is possible that $T_1(T)$ might vary within the unit cell, causing the Mu@C_{60} and ^{13}C to vary differently. The similarity of the temperature dependence of $(T_1T)^{-1}$ for alkali and ^{13}C NMR, though, suggests that any electronic correlation contribution to T_1 does not vary significantly with position in the unit cell in either $Fm\bar{3}m$ (Ref. 100) and $Pa\bar{3}$ (Ref. 101) materials. Even if the hyperfine couplings and $g_N(0)$ were identical, it is possible[104] that different levels of disorder could lead to different values of T_1. Thus we conclude that simple comparison of the magnitudes of T_1 (from μSR or NMR) between nonisostructural A_3 superconductors may not represent a comparison of $g_N(0)$. The possibility that C_{60} polymerization is the source of suppression of the normal state $(T_1T)^{-1}$ is discussed in Sec. VII.

If the T_1 relaxation is *too slow* to be observed, the amplitude of the signal due to Mu, which is field dependent below ~ 0.5 T, can still be used to identify Mu. The field dependence follows:

$$A_{Mu}(B) = A\frac{1+2x^2}{2(1+x^2)}, \tag{5.4}$$

where x is the reduced field B/B_{hyp}, and B_{hyp} is defined as $A_\mu/(\gamma_e+\gamma_\mu)$ (see Sec. 7.3.1 of Schenck[13]). Measurement of this field dependence, when the Mu asymmetry is nonrelaxing, requires careful accounting of the systematic field-dependent shifts in the LF-μSR baseline. This method has the advantage that it admits the possibility of measuring the

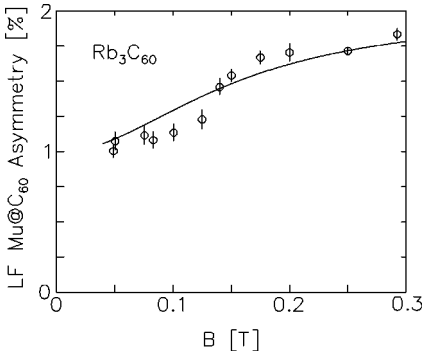

FIG. 10. The LF dependence of the Mu@C_{60} asymmetry (decoupling curve). The field at the inflection point indicates that the Mu hyperfine parameter is large (near its vacuum value). Each point is determined from a common fit to at least two different temperatures, ranging from 2.5 to 15 K (e.g., Fig. 15).

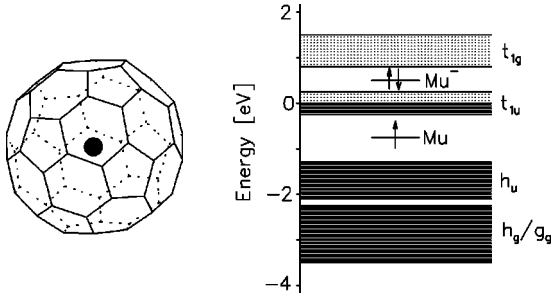

FIG. 11. Endohedral muonium, a 1*s* state at the center of the C_{60} molecule, and the proposed impurity level structure. The Mu^- state is higher in energy because of strong on-site Coulomb repulsion. The T dependence in Fig. 12 may indicate that the Mu^- is considerably lower in energy than shown, and is possibly a resonant state within the t_{1u} conduction band.

hyperfine parameter (although not as accurately as precession) which determines, for example, the inflection point of the decoupling curve Eq. (5.4). We have made two measurements of the LF muonium decoupling curve in two different samples of Rb_3. In the first measurement, we acquired pairs of spectra at 35 and 4 K at each field in a special apparatus which allowed collection of a reference spectrum in high-purity silver in the same conditions of field and temperature *simultaneously*.[105] Systematic shifts in the baseline could thus be at least partially compensated using the reference data. In the second experiment, we took data in various fields at two (or more) temperatures, one where the relaxation was quite fast, and one where it was slow in order to determine the relaxing amplitude, i.e., the muonium asymmetry A_{Mu} (see Fig. 10). The results of this second method are roughly consistent with the first measurement but less scattered. The decoupling in the data is apparently sharper than expected (fit curve). In this data, we did *not* field cool, but the consequent additional inhomogeneity of the field would not affect the decoupling significantly. Any correlation of the amplitude and relaxation rate, due for example to a nonexponential relaxation, could bias the extracted asymmetry and account for the sharper feature. From the fit to Eq. (5.4), we get $A_\mu = 4300(400)$ MHz.

It is remarkable that paramagnetic Mu@C_{60} is stable in a metal such as Rb_3C_{60}. Normally, the conduction electrons in a metallic environment shield the positive charge on the muon such that there is no bound state for a single electron. The situation in C_{60} fullerides is therefore quite unique. The large isotropic hyperfine parameter is close to that for muonium in vacuum implying that the electronic wave function around the muon is very much like the 1*s* state of a hydrogen atom and not changed appreciably from what is observed in the insulating phases. One important factor is that the conduction electrons in Rb_3C_{60} are confined to the region of the carbon shell leaving a cavity inside where there is little conduction electron density. In this situation a positive muon can bind a single electron with minimal disturbance from the conduction electrons. Of course the conduction-electron wave function does extend into the interior of the ball and this is in fact what gives rise to the observed spin-exchange relaxation. Apparently the negative charge state of muonium, which is diamagnetic, does not form due to a large electron repulsion energy (U). This is similar to the negative ion of muonium or hydrogen in which the second electron is bound by only 0.75 eV. The stability of the neutral paramagnetic muonium implies the energy level corresponding to doubly occupied negative charge state of muonium must therefore be above the Fermi level. A level scheme for Mu and Mu^- in Rb_3C_{60} is thus shown in Fig. 11 where the Fermi energy occurs in the center of the t_{1u} band.

The high stability of Mu@C_{60} in Rb_3C_{60} at low temperatures is clearly demonstrated by the Korringa-like relaxation below 100 K. However, at higher temperatures there is evidence for local excitations of some kind since the relaxation rate increases with temperature much faster than the Korringa expression would predict (see Fig. 12). One possibility is that above 100 K one begins to rapidly cycle between Mu^- and Mu. The resulting capture and loss of an electron mimics spin exchange since the spin correlation on the bound electron of muonium is lost after such an event. A similar phenomenon has been used to explain rapid $1/T_1$ spin relaxation in semiconductors at high temperatures.[106] The small activation energy of 588(40) K (see the solid curve in Fig. 12) suggests that the energy level of Mu^- is just above the Fermi energy. Other types of local excitations may be involved, though. For example, one would expect that the first vibrational excitation of Mu@C_{60} to be much more strongly coupled to the conduction electrons, so excitation of such a state could account for the increase in $1/T_1$ as observed.

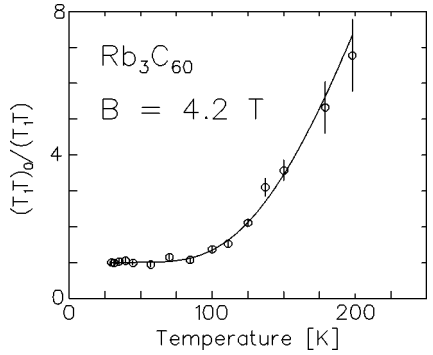

FIG. 12. Activated increase in $(T_1T)^{-1}$ relative to its value at low temperature likely due to Mu@C_{60} ionizing to endohedral Mu^-. The fit curve is $[1.01(3)+123(35)\exp(-588(40)\ \mathrm{K}/T)]$.

In conclusion we note that the important features of the muon sites in the A_3C_{60} superconductors to the analysis included in the following sections are simply that the muons stop randomly on the relevant length scales of the vortex state: the penetration depth λ and the vortex spacing; most of the muons remain diamagnetic and sample the field distribution of the vortex state uniformly; and a small fraction of the muons form a paramagnetic muonium center which is only very weakly coupled to the conduction electrons.

VI. TRANSVERSE FIELD: THE VORTEX STATE FIELD DISTRIBUTION

In TF experiments in A_3C_{60} superconductors, it is found[107–109] that a large fraction of the injected muons remain diamagnetic, and their precession signal is broadened below T_c by the inhomogeneous magnetic field distribution of the vortex state.

The line shape due to the field distribution of a triangular flux-line lattice (FLL) with additional effects due to flux-lattice disorder and anisotropy have been studied in detail in the context of high-T_c superconductors.[110–113] The characteristic features of this line shape can be related to the spatial distribution of fields of the triangular FLL: there is a sharp low-field cutoff of the line shape due to the minimum field that occurs in the center of a triangle defined by three neighboring vortices; at slightly higher field, there is a sharp peak due to the highly weighted field corresponding to the saddle point midway between two vortices; and there is a sharp high-field cutoff due to the maximum field occurring in the vortex cores. For an ordered triangular FLL, it is found that the second moment of the field distribution is related to the London penetration depth at intermediate fields by[110]

$$\lambda \approx \left[3.71\times 10^{-3} \frac{\Phi_0^2}{(\Delta B)^2} \right]^{1/4}, \tag{6.1}$$

where $\Delta B = \sigma_S(0)/2\pi\gamma_\mu$ is the rms deviation of the field distribution.

To accurately determine λ for a perfect triangular FLL, involves more detailed modeling of the field distribution. One such model relies on an approximate low-field solution of the Ginzburg-Landau theory,[114] which, more recently, has been extended to higher fields[115] and further simplified.[116] This theory results in a field-dependent relationship (for $B \ll B_{c2}$),

$$\lambda \approx \left[3.71\times 10^{-3} \frac{\Phi_0^2 f_v^2(B/B_{c2})}{(\Delta B)^2} \right]^{1/4}, \tag{6.2}$$

where f_v is a universal function of order unity (but sharply field dependent) at low reduced fields. λ estimated from Eq. (6.2), for $B/B_{c2} \approx 0.02$, will be ~15% smaller than that of Eq. (6.1). Estimates of λ can be improved by fitting a model of the asymmetric field distribution, rather than just using the second moment.[117,113] If the fractional volume of the FLL corresponding to the vortex cores is large enough, the high–field cutoff will be observable, and the superconducting coherence length ξ can be measured.[118,119]

It would be surprising to find a perfect triangular FLL in powdered superconductors, such as these, where both the vortex separation and λ are on the same scale as ξ_{XTL}, the coherence length of crystalline order. One would instead expect that the flux lattice would be disordered and that the measured magnetic-field distribution would be smeared relative to the perfect FLL. Such smearing would make a significant contribution to the second moment of the field distribution, e.g., see Ref. 112, making the applicability of the above theories questionable. This is just the situation we find [see, for example, Fig. 13(a)]. The line is much broader than in the normal state but exhibits only a slight asymmetry. It is unreasonable to attempt to fit such a smeared line shape to the full theoretical shape, but Fig. 13(b) shows two simulated line shapes for comparison. We note that the fluxoid distribution is *not* melted and only weakly pinned at 3 K and 1 T, because, for example, shifting the applied field at this temperature causes the line to shift in frequency, but broaden significantly. This is in contrast to crystalline $YBa_2Cu_3O_{6.95}$, where[117] shifting the field shifts only the background signal as the FLL is well pinned, and to the vortex-liquid state, where the (symmetric) line simply shifts without altering shape.

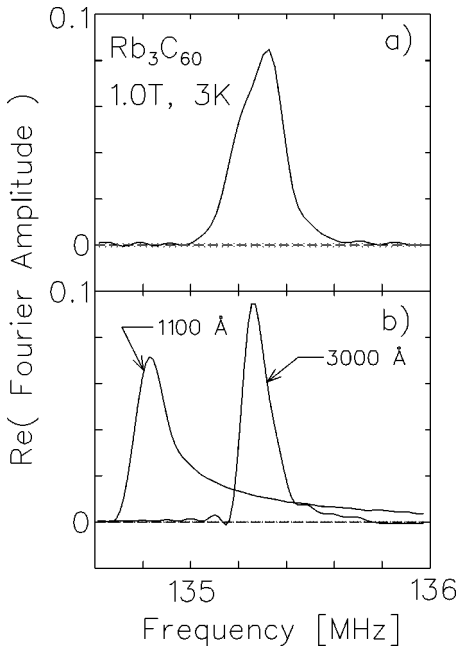

FIG. 13. (a) A high statistics μSR line shape (FFT of TF asymmetry spectrum) in Rb_3C_{60} field-cooled to 3K at 1.0 T applied transverse field. (b) Simulated line shapes for a perfectly ordered triangular flux lattice using the Ginzburg-Landau theory (Refs. 114–116). The simulation parameters (λ,ξ) are (3000 Å, 30 Å) and (1100 Å, 30 Å). The field distributions are convoluted with a Gaussian corresponding to the normal-state linewidth. The 3000 Å simulation also includes a small nonrelaxing background signal known to exist in the data.

Clearly, the 1100 Å value of the penetration depth deduced from magnetization measurements is inconsistent with the observed line shape, since no amount of disorder will narrow the line, and estimates of the correlation time for motion of the vortices from NMR (Ref. 120) suggest that, at low temperatures, there should be no dynamical narrowing of the μSR line. The high-field cutoff in the FLL field distribution will move down towards the average field as *either* λ or ξ increases. Because of this correlation, the absence of

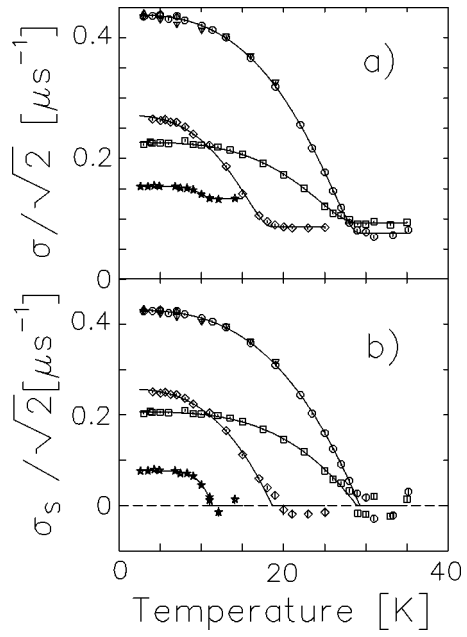

FIG. 14. (a) Second moments of the μSR line shape as a function of temperature in *stars*: Na_2Cs (0.01T), *diamonds* K_3 (1.0T), Rb_3 (*circles* 1.0 T, *triangles* 0.5 T, *nablas* 1.5 T), and *squares* a second sample of Rb_3 (0.27 T). (b) Second moments corrected for the normal-state values.

a long high-frequency tail in the observed line shape [Fig. 13(a)] constrains only the pairs (λ,ξ), i.e., along the line (λ,30 Å) the observed line shape is consistent with λ larger than $\approx$3000 Å with the condition that larger values of λ will require a greater degree of disorder to match the observed linewidth. Such an inconsistency between the magnetization and μSR results is not surprising, since the procedure for obtaining λ from the magnetization is fraught with difficulties[5,2] of which only some are reduced or eliminated through use of a single crystal instead of powder. We note that other results using NMR (Ref. 102) and optical[121] methods also find $\lambda > 3000$ Å.

We extract the second moment from the TF data by fitting the time-dependent envelope of the precession signal to a Gaussian of the form $A\exp(-(\sigma t/\sqrt{2})^2)$. The results are shown in Fig. 14(a). In the normal state, the line shape is a narrow Gaussian whose width is determined by the distribution of magnetic fields due to the randomly oriented nuclear dipoles (^{13}C,^{23}Na,^{39,40,41}K,^{85,87}Rb,^{133}Cs). This normal state width σ_N is temperature independent in the range between T_c and room temperature (except for Na_2Cs, discussed below) and adds in quadrature to the σ_S due to the disordered FLL to determine the overall σ below T_c. We use this correction to produce σ_S shown in Fig. 14(b). The temperature dependences are fit to the phenomenological form $\sigma_S(0)[1-(T/T_c)^{\varpi}]$, and the resulting parameters are given in Table II. In spite of the lack of the signature of the FLL in the line shape, we expect that the overall linewidth is controlled by λ (and much more weakly by ξ) and that $(\Delta B)^{-1/2}$ will scale with λ. We have calculated the values λ reported in Table II using the linewidths $\sigma_S(0)$ and Eq. (6.1). Because of the increase of ΔB from disorder of the FLL, this conversion will *underestimate* the actual λ, so this, or perhaps more conservatively the value from the field-dependent theory (which we have not included because of uncertainty in the value of B_{c2}), should be considered a *lower bound* for λ. These results can be compared directly with those of Refs. 107,108. Note that at low temperature, $\sigma_S(T)$ is quite flat in contrast to the *d*-wave linear-*T* dependence seen in *clean* high-T_c,[122] suggesting that, in this respect, the A_3C_{60} superconductors appear conventional. This conclusion is not strong, however, because in *d*-wave systems, for example, impurity scattering can lead to[123] a weaker low-*T* dependence of λ. In Rb_3, there is no apparent field dependence to $\sigma_S(T)$ between 0.5 and 1.5 T, so the applicability of Eq. (6.2) is questionable. Furthermore, there is large sample dependence of σ_S in Rb_3 suggesting a strong effect of disorder on λ. In the dirty limit $\xi \approx l$, where l is the electron mean free path. The penetration depth varies sensitively with l via

$$\lambda^{-2} \propto \frac{n_s}{m^*}\frac{1}{1+\xi/l}, \tag{6.3}$$

where n_s is the superelectron density and m^* is the effective conduction-electron mass. Thus if l is on the same order as the coherence length, any sample-dependent disorder that contributes to l could alter λ. The low T dependence of σ_S has been fit to the BCS activated form[35] for the clean limit;[109] however, the dirty-limit form is probably appropriate to Rb_3 and K_3 (but possibly not to Na_2Cs). In this case,[34] for $T < 0.5T_c$,

$$\sigma_S \approx \sigma_{S0}[1+e^{-\Delta_0/kT}]^{-2}, \tag{6.4}$$

where Δ_0 is the low-temperature BCS gap parameter. The results of these fits are also given in Table II. We note that some caution must be taken regarding the interpretation of the TF results for Na_2Cs because (i) the applied field was very low (not far from H_{c1}) and (ii) σ_N was rather large and temperature dependent above 50 K. The behavior of $\sigma_N(T)$ may be associated with molecular dynamics and/or a small fraction of the muons stopping in unmasked areas of the Al

TABLE II. Parameters of the TF linewidth fits described in the text and shown in Fig. 14. The numbers in brackets after the sample indicate the applied field in each case. ΔB is the rms width of the field distribution. Δ_0/kT_c is obtained from fits to Eq. (6.4) and the T_c values in the table.

Sample [B (T)]	$\sigma_N/\sqrt{2}$ (μs^{-1})	$\sigma_S(0)/\sqrt{2}$ (μs^{-1})	T_c (K)	ϖ	ΔB (mT)	λ (Å)	Δ_0/kT_c
Rb_3C_{60}-1(1.0)	0.076(1)	0.4315(10)	29.3(8)	2.93(4)	0.717	4200	1.37(5)
Rb_3C_{60}-2(0.27)	0.093(1)	0.2068(10)	28.9(2)	3.36(8)	0.343	6100	1.56(5)
K_3C_{60}(1.0)	0.087(1)	0.2570(20)	18.6(2)	2.83(9)	0.427	5400	1.39(6)
Na_2CsC_{60}(0.01)	0.133(1)	0.0769(10)	11.3(3)	7.5(1.0)	0.128	9900	

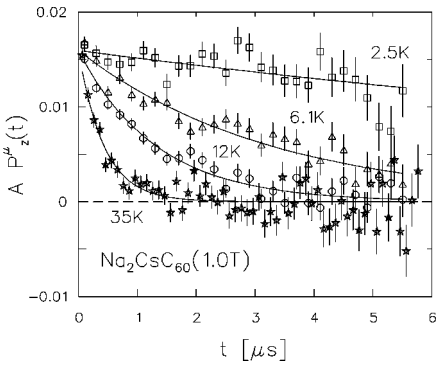

FIG. 15. Single exponential relaxation of Mu@C_{60} in Na_2CsC_{60} in a longitudinal applied field of 1.0 T. The fits shown are to a common amplitude exponential relaxation.

sample cell. However, the observed σ_S agrees with another published measurement[108] at higher field indicating that the field dependence is not appreciable. Furthermore, any Al signal will make no contribution to the signal in high LF discussed in the following section.

The historic evolution of μSR measurements of λ in $YBa_2Cu_3O_{6.95}$ may provide a guide for the robustness of estimates of λ from the second moment of the μSR line shape. Despite the more serious consequences of powder averaging in these highly anisotropic systems, the extracted penetration depth from μSR data [even from symmetric line shapes, like Fig. 13(a)] has exhibited a variation of only $\sim$30% (including model as well as sample variation). Thus the most serious uncertainty with our determination of λ may be the strong sample dependence. The observation of the asymmetric line shape characteristic of a triangular FLL would certainly make our conclusions much stronger, and such line shapes are expected in single crystals which can now be made in sufficient size[3] for such an experiment.

We turn now to the temperature dependence of the LF (T_1) relaxation of Mu@C_{60}, noting that the interstitial diamagnetic muons will not contribute to this signal except at (LF) magnetic fields less than a few mT.

VII. LONGITUDINAL FIELD: T_1 RELAXATION OF Mu@C_{60}

The relaxation of Mu@C_{60} in high LF ($B \geqslant 0.75$ T) is found to be single exponential, e.g., Fig. 15. The relaxation rates exhibit essentially temperature-independent $(T_1T)^{-1}$ behavior between about 50 K and T_c for each of the systems, Rb_3, K_3, and Na_2Cs. In Rb_3 we find no sample dependence, but in Na_2Cs we find a significant difference between two runs on the same sample which we interpret as evidence for a second low-temperature phase, the formation of which is quench-rate dependent. We thus postpone discussion of the temperature dependence in Na_2Cs to Sec. VII B.

A. $T_1(T)$ in Rb_3 and K_3

The average normal-state values of $(T_1T)^{-1}$ are shown in Fig. 9(b). At higher temperature there are deviations (Fig. 12), but at low temperature, we have no significant evidence for previously reported[17] weakly non-Korringa behavior. Just below T_c, for $B \approx 1-2$ T, we find a slightly enhanced

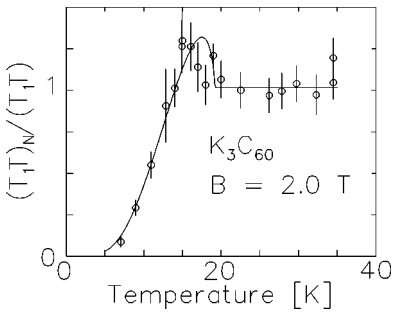

FIG. 16. Temperature dependence of the spin-relaxation rate of Mu@C_{60} in K_3C_{60} at a field of 2.0 T. The fit is to the Hebel-Slichter integral Eq. (4.4) with a broadened DOS of the form Eq. (4.7).

$(T_1T)^{-1}$ followed by an strong falloff below about $0.75T_c$. An example of this is shown in Fig. 16, where the LF relaxation rate divided by the linear normal-state temperature dependence is plotted (normalized). This ratio is just the ratio R_S/R_N discussed in Sec. IV.

We find that increasing the disorder in the FLL in Rb_3 does not affect the peak height by comparing field-cooled and zero-field-cooled $(T_1T)^{-1}$ at the peak temperature, T_P, at 1.5 T. However, we find, in Rb_3, that the peak is strongly field dependent (similar behavior was independently discovered in NMR T_1 measurements in Rb_2CsC_{60} by Stenger[100]). It is suppressed as the field is increased above about 2 T, and is entirely gone by 4.2 T (Fig. 17). The observed heights of the peaks from fits to a parabola near T_P are shown in Fig. 18.

In order to discuss analysis of the peaks in terms of the theory outlined in Sec. IV, we include some brief remarks about the DOS functions used. First we note g_D and g_{SC} [Eqs. (4.7) and (4.8)] do not depend on the sign of the broadening parameter (Γ or Δ_2), which we take to be positive.

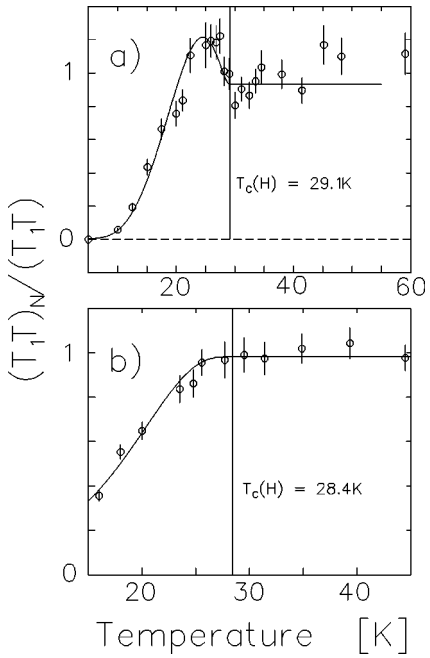

FIG. 17. Magnetic-field damping of the Hebel-Slichter peak in Rb_3C_{60}; note the different temperature scales. The longitudinal fields are (a) 1.5 T and (b) 4.2 T.

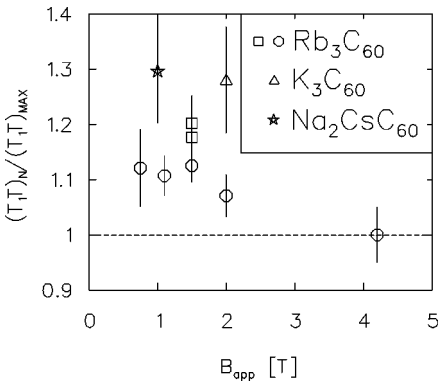

FIG. 18. Heights of the coherence peak above the normal state as a function of field. These values were obtained from fits to a parabola near the maximum. The suppression of the coherence peak by magnetic field is much stronger than that observed in the conventional type-II superconductor V_3Sn (Ref. 84).

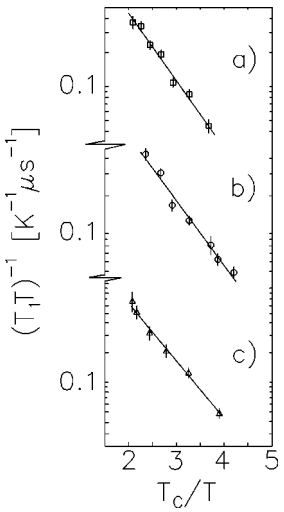

FIG. 19. The temperature dependence of $(T_1T)^{-1}$ at 0.3 T at low reduced temperature. (a) and (b) two samples of Rb_3, and (c) K_3. The temperature dependence is activated, but the value of the energy gap depends on the model of the superconducting density of states, g_S. The energy gap values for various models are discussed in the text.

The property of conservation of the total number of electron states, which simply results from the construction of the eigenstates of the superconductor from those of the normal state, can be succinctly written,

$$\int_0^\infty [g_S - g_N] dE = 0. \tag{7.1}$$

The BCS g_S follows this, as does the heuristic form g_D; however, the strong-coupling form g_{SC} Eq. (4.8) does not; in fact,

$$\int_0^\infty [g_{SC} - g_N] dE = -|\Delta_2|, \tag{7.2}$$

i.e., there are effectively fewer states in g_{SC} than in the normal state. Of course, in the full strong-coupling theory, $\Delta = \Delta(E,T)$, g_{SC} will have structure above the gap, and Eq. (7.1) will be obeyed. One consequence of this property of g_{SC}, is that the integral for $(T_1T)^{-1}$ Eq. (4.4) will approach a value less than 1 as T approaches T_c from below. The resulting discontinuity scales with Δ_2, and is negligible for small Δ_2. However, if g_{SC} is used to model the small coherence peaks reported here, Δ_2 is relatively large, and the discontinuity is significant, so that the approximation introduced by Fibich,[51] that the energy dependence of Δ_2 can be neglected in calculating the coherence peak seems untenable in the current context, and in order to use strong-coupling results, one would have to resort to more detailed calculations.[54,46] There is also a significant difference between g_D and g_{SC} in the limit $E \to 0$, which is important in determining the low-temperature behavior of $(T_1T)^{-1}$: $g_D(0) = [1 + (\Delta/\Gamma)^2]^{-1/2}$, while $g_{SC}(E)$ goes to zero with slope $\approx |\Delta_2|/\Delta_1$ as $E \to 0$.

The low-field peaks have been fit to Eq. (4.4) using both the DOS functions g_D and g_{SC} (avoiding the discontinuity mentioned above by only considering the data below T_c) with $\mathrm{Re}\{\Delta\} \propto \Delta_{\mathrm{BCS}}(T)$, which is still quite a good assumption in the strong-coupling case.[47] We find that, in order to explain such a small height of the coherence peak, the broadening parameters near T_c must be $\Gamma/\Delta_0 \approx \Delta_2/\Delta_0 \approx 10\%$. If the broadening is due to strong electron-phonon scattering, then it should be significantly temperature dependent. For a Debye phonon spectrum, at low temperature, $\Delta_2 \propto T^{7/2}$. The contribution of the low-energy libron peak[124] may modify this somewhat; although, weak electron coupling to this mode will limit its effect. The results of tunneling experiments could, in principle, provide confirmation of the sharpening of g_S at low temperature, but the published spectra are rather equivocal: low-temperature break-junction tunneling spectra show rather broad peaks,[4] while point-contact spectra are quite sharp[125] and other STM measurements are fairly broad but show a strong dependence on crystallinity.[126] Recent planar junction tunneling measurements[127] confirm the former behavior, suggesting an intrinsic nearly temperature-independent broadening mechanism for g_S. The width of the coherence peak is controlled by the balance between the peak contribution to the integral Eq. (4.4) and the exponential behavior due to the opening of the gap; thus, there is significant correlation between the value of Δ_0 and the temperature dependence of the broadening parameter. Generally, a broadening that falls off steeply as the temperature decreases causes the peaks of g_S to sharpen, and the coherence peak to widen; consequently, the value of Δ_0 required to explain the observed peak width will be larger than for a broadening which is more weakly T dependent.

In high field T_1^{-1} becomes too slow to observe at low reduced temperature, so we use the strong field dependence [Eq. (3.4) and Fig. 9] and study this region in a reduced applied field. In this case, over the temperature range $0.5T_c$–$0.25T_c$, $(T_1T)^{-1}$ exhibits activated behavior as shown in Fig. 19. Again the values of Δ_0 required to fit this data depend on what broadening is assumed at low temperature. Because of the Fermi factor in the integral Eq. (4.4), the low-temperature behavior of $(T_1T)^{-1}$ is determined mainly by the gap and contains no information about the shape of the broadened DOS peaks. However, if there are states within the gap, the temperature dependence may deviate strongly from the activated temperature dependence. We have fit the low-temperature data to the same set of models

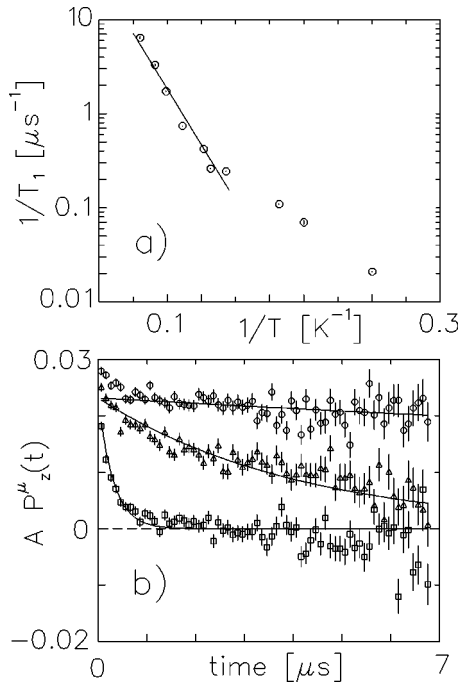

FIG. 20. Residual relaxation at low reduced temperature in Rb_3 in a LF of 0.3 T. (a) The temperature dependence deviates from the activated behavior at higher temperature (line). (b) The relaxation at 4 K (circles), 7 K (triangles), and 11 K (squares). The data at 4 K show a very small fast relaxing component at early time. This signal is likely related to disorder and not to the vortex cores.

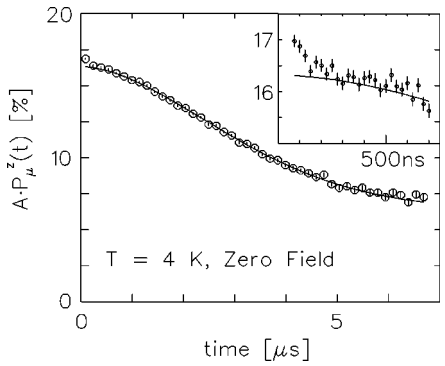

FIG. 21. A high statistics zero applied field time spectrum in the Meissner state of Rb_3C_{60} at 4 K. The slow Gaussian relaxation is likely due to the diamagnetic interstitial muons relaxing in the distribution of magnetic fields of the randomly oriented static nuclear dipoles, while the small fast relaxing component (inset) is attributed to relaxation of the endohedral $Mu@C_{60}$. Both dynamic and static random magnetic fields can contribute to this relaxation. Dynamic fields could be due to remnant states within the gap as seen in finite low-temperature zero-bias conductance in several tunneling experiments.

as the peak data at higher field. Two cases for the temperature dependence of the broadening assumed: strong ($\approx T^{7/2}$) and temperature-independent broadening, noting that the real dependence will likely lie somewhere in this range. The results are as follows: for the strongly temperature-dependent broadening, the high-field data require large $2\Delta/kT_c$ ($\approx$4.5), but the low-field data at low temperature require a near weak-coupling value. Much better agreement in the value of $2\Delta/kT_c$ between the high- and low-field data is obtained assuming a weakly temperature dependent g_S broadening. In this case, $2\Delta/kT_c$ is in the range 3.5–4.0.

In Rb_3 at 0.3 T we find at lower temperatures a sample-dependent residual relaxation that is much more weakly temperature dependent (Fig. 20). The source of this residual relaxation could be related to crystalline disorder (in alkali site occupation or degree of orientational disorder) and the finite low-T zero-bias conductance observed in tunneling (zero applied magnetic field). There is also evidence that the C_{60} molecules in $Fm\bar{3}m$ phases undergo orientational dynamics which freeze out near or below room temperature.[6] Thus, it is possible that the degree of orientational disorder varies with cooling procedure. We have attempted no systematic quench-rate dependences, but there is some evidence that the low-T residual relaxation *and* the large sample dependence of λ may be partially due to different cooling procedures. We note that there is no evidence in the $Fm\bar{3}m$ materials for a low-T polymerized phase, which occurs only for intercalated C_{60} materials with smaller cubic lattice parameters such as Na_2A. The superconducting transition in K_3 is extremely sensitive to radiation-damage-induced disorder.[128] Such behavior may be a consequence of the narrow conduction band. If this is the case, then variation of quenched disorder may also have an unusually large effect. At finite field another source of this relaxation could be the vortex cores (Sec. IV D). The relaxation rate of the small fast relaxing component is roughly that of the (extrapolated) normal material, but the amplitude is too large for the small ($\xi = 30$ Å) cores. Moreover, it does not appear to change linearly in amplitude with field near 0.3 T (see Sec. IV D). On the other hand, the linear field dependence would be rather difficult to observe because of the intrinsic field dependence of the relaxation rate and the extremely small amplitude. The persistence of some relaxation at low temperature in zero applied field (inset, Fig. 21) suggests that at least some of this residual relaxation is not due to vortices. The relaxation in zero field, however, can have contributions from both static and dynamic fields.

The small size of the coherence peak is not the result of the perturbing influence of the paramagnetic Mu atom. While it has recently been shown that single paramagnetic atoms locally perturb the surrounding superconductor,[129] the Mu as shown in Sec. V is only very weakly coupled to the conduction electrons. The strong evidence that the Mu perturbation is small is the agreement of the temperature dependence of $(T_1T)^{-1}$ with similar NMR experiments.[23] On the other hand, the suppression of the peak can be due to any of the mechanisms discussed in Sec. IV C or a combination of these mechanisms. Recent tunneling measurements suggest that we should expect some broadening from strong-coupling effects. We expect at most a *small* amount of anisotropy [large anisotropy is not appropriate to explain either the low-temperature behavior of the TF linewidth σ or $(T_1T)^{-1}$]. Also, because the $Fm\bar{3}m$ materials are likely in the extreme dirty limit ($l < \xi$) anisotropy would be eliminated by electron scattering.[33] However, the strong field dependence of the coherence peak is not accounted for explicitly by either of these mechanisms, so we now consider the effect of magnetic field introduced in Sec. IV D. The observed suppression of the

peak by magnetic field occurs in a very different part of the phase diagram than regions (i) and (ii) of Fig. 7, where it is certainly expected, so that the gaplessness due to proximity to H_{c2} does not account for the observed damping. However, we note that some H_{c2} measurements by magnetization exhibit unusual temperature dependence[2] near $T_c(0)$. Our measurements of $T_c(H)$ via TF μSR (Table II), though, are consistent with a strongly T-dependent H_{c2} near $T_c(0)$. We have assumed such a strong T dependence to arrive at the estimate of $T_c(4.2\ \mathrm{T})$ in Fig. 17(b). We expect that the effects of Pauli pair breaking on the coherence peak will also be small because, as the Yosida function behavior of the NMR Knight shift[23] shows, spin-orbit scattering is very weak in these materials. The crude model used to explain the NMR coherence peak[23] [i.e., Eq. (4.13)] does not satisfactorily explain the damping observed in μSR or NMR. For example, in Fig. 17(a) at 20 K, the value of $(T_1T)^{-1}$ is near its value in the normal state, so no weighted average of $(T_1T)^{-1}$ with its value in the normal state will give the observed value at roughly the same reduced temperature at 4.2 T of $\sim 0.6\ (T_1T)_N^{-1}$. Furthermore, this model (which treats the vortices as normal cylinders) is expected to apply[72] only when $B \ll B_{c2}$. The observed strong suppression of the coherence peak occurs in the nonlinear region of the phase diagram and may be explained by more detailed theories.[73,76] The detailed mechanism for this suppression could be elucidated by STM measurements which can resolve both the spatial and energy dependences of the superconducting DOS.

B. $T_1(T)$ and quench rate dependence in Na_2Cs

In two separate measurements on the *same sample* of Na_2Cs, we observed very different behavior. In the initial run, we found no broadening of the TF precession signal associated with T_c. We did, however, observe the expected Mu@C_{60} T_1 relaxation. The temperature dependence of this relaxation rate remained Korringa-like [Fig. 22(a)] down to about 8 K, below which it began to increase. To ensure that the sample had not deteriorated, it was recharacterized by x-ray diffraction after this run. In the subsequent run, we observed T_c in TF (Fig. 14) and in LF [Fig. 23(a)]. Because of the low temperature of the structural phase transition in this material[130] (299 K), we suspected a quench-rate dependence, possibly due to frozen orientational disorder. We attempted a fast quench (sample at 300 K for 20 min, then quenched to 200 K in 5.5 m and to 5 K in about 20 min), and found that this cooling procedure did not affect the height of the coherence peak, but it did reduce the low-temperature T_1 rates at 2.7 K in both 1 and 0.3 T (stars in Fig. 23). However, with no evidence at the time for ambient pressure polymerization, we did not attempt a slow quench or anneal, and, only for the last three points, did we record the cooling procedure in sufficient detail. It now seems likely that, as in the case of Na_2Rb, there exists another stable ambient pressure low-temperature phase of Na_2Cs, which may involve C_{60} polymerization. According to our measurements (Fig. 22) this phase is metallic, nonsuperconducting and appears to exhibit a low-temperature (possibly magnetic) phase transition. We note that attempts by another group have not produced an ambient pressure polymerized phase in Na_2Cs.[62] The unusually small value of $(T_1T)^{-1}$ in Na_2Cs (discussed in Sec. V) *cannot* be explained by the coexistence of the superconducting (s–Na_2Cs) and nonsuperconducting (ns–Na_2Cs) phases, as the values of $(T_1T)^{-1}$ are indistinguishable except below ~ 8 K. However, as the fast-quench procedure suggests, a small fraction of the nonsuperconducting phase could explain the finite low-temperature rate in

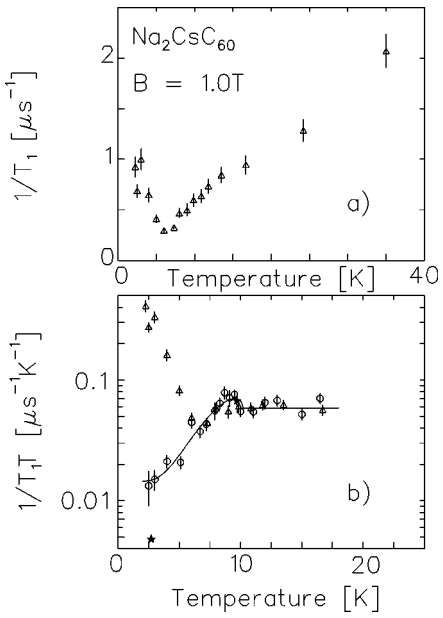

FIG. 22. Quench-rate dependence of the Mu@C_{60} T_1 relaxation rate in Na_2CsC_{60}. *triangles*: nonsuperconducting run, *circles*: superconducting run, *stars*: fast quench. Note that above about 10 K, the values of T_1T in both runs are about the same. The line is the same fit as in Fig. 23(a).

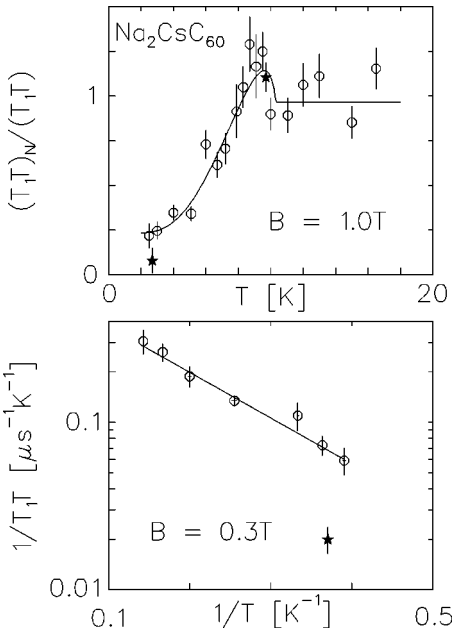

FIG. 23. The coherence peak and low-temperature falloff in superconducting Na_2Cs. The solid stars indicate fast quench runs (described in the text). The low-temperature fast-quench values indicate that the activated dependence is probably weakened by partial polymerization, and that the intrinsic temperature dependence in the superconducting phase is probably much stronger.

Fig. 23. The field dependence of T_1^{-1} in the ns-Na_2Cs was also indistinguishable from the superconductor at 35 K [Fig. 9(a)], but at 3 K, appeared to fall more sharply with field. In addition there was a small peak in the linewidth of the diamagnetic precession at $\sim$7.5 K in ns-Na_2Cs. The weak low-T dependence of the diamagnetic signal compared to the T_1 of Mu@C_{60} is consistent with the enhanced sensitivity of Mu due to the bound electron moment. One possible explanation for the feature in TF, is that ns-Na_2Cs is superconducting over a narrow range in temperature, and is re-entrant at about 7 K to a low-temperature nonsuperconducting phase.

Despite the complications due to the presence of some fraction of ns-Na_2Cs in the superconducting run, we can compare the temperature dependence of T_1 with the cubic $Fm\bar{3}m$ materials discussed above. In order to account for an ns-Na_2Cs fraction, we model $(T_1T)^{-1}$ as the sum of the Hebel-Slichter integral Eq. (4.4) with an additional T-independent term. Such fits are shown in Fig. 23.

The fast-quench points indicate that for s-Na_2Cs, values of Δ from the relatively weak temperature dependence of $(T_1T)^{-1}$ (see Fig. 23) would not be reliable. The size of the coherence peak, relative to the normal state, though, is not dramatically different than in the $Fm\bar{3}m$ materials. This implies that orientational disorder is not likely to be the cause of the broadening of the coherence peak (or g_S).

These results clearly indicate the need for further experiments on Na_2Cs with careful attention paid to the cooling procedure. The rapid-quench points suggest that one should be able to make a much more reliable estimate of the parameters of s-Na_2Cs. It also seems likely that in order to study ns-Na_2Cs, it will probably be necessary to investigate temperatures lower than those accessible by pumped liquid-helium cryostats.

VIII. CONCLUSION

In conclusion we have observed the LF relaxation of Mu@C_{60} in the A_3C_{60} superconductors. The temperature dependence of the relaxation rates exhibits Korringa behavior above T_c and a small strongly field-dependent coherence peak and strong activated behavior in the superconducting state. The superconducting energy gap can be extracted from the low-temperature behavior. A large uncertainty in the gap measurement comes from uncertainty in the appropriate form of the temperature-dependent superconducting DOS. For Rb_3 and K_3 and the range of models considered, the reduced gap $2\Delta/kT_c$ lies in the range 2.4–4.8. However, for consistency between the high- and low-field temperature dependences, a weakly temperature-dependent broad DOS is favored, and the reduced gap values lie between 3.2 and 4.0. The upper end of this range as well as the broad low-temperature DOS peaks are consistent with the tunneling and optical results of Köller.[4] The small size of the peak can be due to one or several factors, such as the moderately strong electron-phonon coupling suggested, for example, by tunneling.[4,127] Following Pennington and Stenger[23] we conclude that, provided the results of Akis[54] carry over directly to the case of A_3C_{60}, which possesses a very broad and complicated phonon spectrum, the small size of the 1.5 T coherence peak implies $T_c/E_{\ln}\approx 0.2$. A ratio as large as this is incompatible with the near weak-coupling value of the energy gap which gives[4] $T_c/E_{\ln}<0.1$. Thus strong coupling alone will not consistently account for the both the small coherence peak and the gap. Together with the strong field dependence of the coherence peak, this suggests that an additional coherence peak suppression mechanism connected with the inhomogeneous vortex state must be present. A full explanation of such an effect would require extension of the theories discussed in Sec. IV D (Refs. 73,76) to the regime of strong coupling.

In transverse field we find broadening of the μSR precession line due to the inhomogeneous fields of the vortex state. There is no clear flux-lattice line shape, so we can only estimate the magnitude of λ, which for example in Rb_3 lies in the range 3000–7000 Å. This range is definitely inconsistent with the values of Chu and McHenry,[3] and this discrepancy is likely not due to sample dependence of λ, but rather to the systematic differences between the two techniques.

A much weaker activated dependence in s-Na_2Cs is attributed to coexistence of a nonsuperconducting phase of Na_2Cs. Quench-rate dependent experiments may be able to clarify this and allow measurement of the properties of both phases. By comparing the coherence peak in $Fm\bar{3}m$ materials with s-Na_2Cs, we find no evidence for an effect on the coherence peak due to the degree of molecular order. In the $Fm\bar{3}m$ materials, quench-rate dependence would also help to clarify the role of frozen orientational disorder in the value of λ and in the residual low-temperature T_1 relaxation.

Finally we note that there are interesting aspects of Mu@C_{60} in A_3 such as its stability and very weak interaction with the conduction band that suggest further theoretical investigation of the detailed properties of endohedral fullerene species.

ACKNOWLEDGMENTS

We would like to acknowledge helpful discussions of various parts of this work with I. K. Affleck, J. P. Carbotte, M. Larkin, G. M. Luke, D. E. MacLaughlin, R. I. Miller, J. Ostrick, P. W. Percival, J. Sagi, and P. C. E. Stamp. We thank K. Prassides for sending us his recent preprints and C. Ballard, M. Good, the staff of the machine shops of TRIUMF and UBC and the TRIUMF scintillator shop for technical support. We also acknowledge P. W. Stephens for assistance in the x-ray characterization of some samples. This work was supported by the Canadian NRC and NSERC. The work at the University of Pennsylvania was supported by U.S. Department of Energy, Grant No. DE-FC02-86ER45254.

*Present address: Laboratoire de Physiques des Solides, 91405, Orsay, Cedex, France.
[1] O. Gunnarsson, Rev. Mod. Phys. **69**, 575 (1997).
[2] V. Buntar and H. W. Weber, Supercond. Sci. Technol. **9**, 599 (1996).
[3] S. Chu and M. E. McHenry, Phys. Rev. B **55**, 11 722 (1997).
[4] D. Köller, M. C. Martin, L. Mihály, G. Mihály, G. Oszlányi, G. Baumgartner, and L. Forró, Phys. Rev. Lett. **77**, 4082 (1996).
[5] A. Ramirez, Supercond. Rev. **1**, 1 (1994).
[6] Y. Yoshinari, H. Alloul, V. Brouet, G. Kriza, K. Holczer, and L. Forró, Phys. Rev. B **54**, 6155 (1996).
[7] K. Prassides, C. Christides, I. M. Thomas, J. Mizuki, K. Tanigaki, I. Hirosawa, and T. W. Ebbesen, Science **263**, 950 (1994).
[8] K. Prassides, K. Vavekis, K. Kordatos, K. Tanigaki, G. M. Bendele, and P. W. Stephens, J. Am. Chem. Soc. **119**, 834 (1997); L. Christofolini, K. Kordatos, G. A. Lawless, K. Prassides, K. Tanigaki, and M. P. Waugh, Chem. Commun. (Cambridge) **1997**, 375.
[9] A. M. Rao, P. Zhou, K. Wang, G. T. Hager, J. M. Holden, Y. Wang, W. T. Lee, X. Bi, P. C. Eklund, D. S. Cornett, M. A. Duncan, and I. J. Amsten, Science **259**, 955 (1993).
[10] O. Chauvet, G. Oszlànyi, L. Forró, P. W. Stephens, M. Tegze, G. Faigel, and A. Jànossy, Phys. Rev. Lett. **72**, 2721 (1994).
[11] P. W. Stephens, G. Bortel, G. Faigel, M. Tegze, A. Jànossy, S. Pekker, G. Oszlànyi, and L. Forró, Nature (London) **370**, 636 (1994).
[12] Q. Zhu, Phys. Rev. B **52**, R723 (1995).
[13] A. Schenck, *Muon Spin Rotation Spectroscopy* (Hilger, Bristol, 1985).
[14] S. F. J. Cox, J. Phys. C **20**, 3187 (1987).
[15] J. H. Brewer, in *Encyclopedia of Applied Physics*, edited by George L. Trigg and Edmund H. Immergut (Wiley-VCH, Weinheim, 1994), Vol. 11.
[16] C. L. Lin, T. Mihalisin, N. Bykovetz, Q. Zhu, and J. E. Fischer, Phys. Rev. B **49**, 4285 (1994).
[17] R. F. Kiefl, W. A. MacFarlane, K. H. Chow, S. Dunsiger, T. L. Duty, T. M. S. Johnstone, J. W. Schneider, J. Sonier, L. Brard, R. M. Strongin, J. E. Fischer, and A. B. Smith III, Phys. Rev. Lett. **70**, 3987 (1993).
[18] B. D. Patterson, Rev. Mod. Phys. **60**, 69 (1988).
[19] J. Korringa, Physica (Amsterdam) **16**, 601 (1950).
[20] C. P. Slichter, *Principles of Magnetic Resonance* (Springer, Berlin, 1990).
[21] L. C. Hebel and C. P. Slichter, Phys. Rev. **113**, 1504 (1959).
[22] However, T_1 can become short enough to observe in semimetals such as graphite [J. A. Chakhalian *et al.*, Hyperfine Interact. **106**, 245 (1997)] and antimony [T. M. S. Johnstone *et al.*, Hyperfine Interact. **106**, 71 (1997)] where the presence of a local electronic moment at the muon is permitted by weaker screening of the muon's Coulomb potential.
[23] C. H. Pennington and V. A. Stenger, Rev. Mod. Phys. **68**, 855 (1996).
[24] Y. Maniwa, T. Saito, A. Ohi, K. Mizoguchi, K. Kume, K. Kikuchi, I. Ikemoto, S. Suzuki, Y. Achiba, M. Kosaka, K. Tanigaki, and T. Ebbesen, J. Phys. Soc. Jpn. **63**, 1139 (1994).
[25] Y. N. Molin, K. M. Salikhov, and K. I. Zamaraev, *Spin Exchange* (Springer, Berlin, 1980).
[26] V. G. Nosov and I. G. Yakovleva, Sov. Phys. JETP **16**, 1236 (1963); M. Senba, J. Phys. B **24**, 3531 (1991).
[27] K. H. Chow, R. L. Lichti, R. F. Kiefl, S. Dunsiger, T. L. Estle, B. Hitti, R. Kadono, W. A. MacFarlane, J. W. Schneider, D. Schumann, and M. Shelley, Phys. Rev. B **50**, 8918 (1994).
[28] S. K. Estreicher, C. D. Latham, M. I. Heggie, R. Jones, and S. Öberg, Chem. Phys. Lett. **196**, 311 (1992); P. W. Percival and S. Wlodek, *ibid.* **196**, 317 (1992).
[29] R. F. Kiefl, T. L. Duty, J. W. Schneider, A. MacFarlane, K. Chow, J. W. Elzey, P. Mendels, G. D. Morris, J. H. Brewer, E. J. Ansaldo, C. Niedermayer, D. R. Noakes, C. E. Stronach, B. Hitti, and J. E. Fischer, Phys. Rev. Lett. **69**, 2005 (1992).
[30] R. F. Kiefl, J. W. Schneider, A. MacFarlane, K. Chow, T. L. Duty, T. L. Estle, B. Hitti, R. L. Lichti, E. J. Ansaldo, C. Schwab, P. W. Percival, G. Wei, S. Wlodek, K. Kojima, W. J. Romanow, J. P. McCauley, Jr., N. Coustel, J. E. Fischer, and A. B. Smith, III, Phys. Rev. Lett. **68**, 1347 (1992); **68**, 2708 (1992).
[31] M. Tinkham, *Introduction to Superconductivity* (McGraw-Hill, New York, 1996).
[32] J. Bardeen, L. N. Cooper, and J. R. Schrieffer, Phys. Rev. **108**, 1175 (1957).
[33] D. E. MacLaughlin, in *Solid State Physics: Advances in Research and Applications*, edited by H. Ehrenreich, F. Seitz, and D. Turnbull (Academic, New York, 1976), Vol. 31, p. 1.
[34] J. Halbritter, Z. Phys. **243**, 201 (1971).
[35] B. Muhlschlegel, Z. Phys. **155**, 313 (1959).
[36] G. Preosti, H. Kim, and P. Muzikar, Phys. Rev. B **50**, 1259 (1994); R. Fehrenbacher and M. R. Norman, *ibid.* **50**, 3495 (1994).
[37] H. Monien and D. Pines, Phys. Rev. B **41**, 6297 (1990).
[38] J. Annett, N. Goldenfeld, and S. R. Renn, in *The Physical Properties of High Temperature Superconductors*, edited by D. M. Ginsberg (World Scientific, Singapore, 1990), Vol. 2, p. 571.
[39] C. H. Pennington and C. P. Slichter, in *The Physical Properties of High Temperature Superconductors* (Ref. 38), p. 269.
[40] J. A. Martindale, S. E. Barrett, C. A. Klug, K. E. O'Hara, S. M. DeSoto, C. P. Slichter, T. A. Friedmann, and D. M. Ginsberg, Phys. Rev. Lett. **68**, 702 (1992).
[41] K. Asayama, Y. Kitaoka, and Y. Kohori, J. Magn. Magn. Mater. **76-77**, 449 (1988).
[42] D. E. MacLaughlin, C. Tien, W. G. Clark, M. D. Lan, Z. Fisk, J. L. Smith, and H. R. Ott, Phys. Rev. Lett. **53**, 1833 (1984).
[43] M. Takigawa, H. Yasuoko, and G. Saito, J. Phys. Soc. Jpn. **56**, 873 (1987).
[44] L. C. Hebel, Phys. Rev. **116**, 79 (1959).
[45] R. C. Dynes, V. Narayanamurti, and J. P. Garno, Phys. Rev. Lett. **41**, 1509 (1978).
[46] P. B. Allen and D. Rainer, Nature (London) **349**, 396 (1991).
[47] J. P. Carbotte, Rev. Mod. Phys. **62**, 1027 (1990).
[48] D. J. Scalapino, in *Superconductivity*, edited by R. D. Parks (Dekker, New York, 1969), Vol. 1, p. 449.
[49] J. R. Schrieffer, D. J. Scalapino, and J. W. Wilkins, Phys. Rev. Lett. **10**, 336 (1963).
[50] S. B. Kaplan, C. C. Chi, D. N. Langenberg, J. J. Chang, S. Jafarey, and D. J. Scalapino, Phys. Rev. B **14**, 4854 (1976).
[51] M. Fibich, Phys. Rev. Lett. **14**, 561 (1965); **14**, 621 (1965).
[52] D. J. Scalapino and T. M. Wu, Phys. Rev. Lett. **17**, 315 (1966).
[53] B. W. Statt, Phys. Rev. B **42**, 6805 (1990).
[54] R. Akis, C. Jiang, and J. P. Carbotte, Physica C **176**, 485 (1991).
[55] H. Y. Choi and E. J. Mele, Phys. Rev. B **52**, 7549 (1995).
[56] A. A. Abrikosov and L. P. Gor'kov, Sov. Phys. JETP **12**, 1243 (1961).
[57] A. Griffin and V. Ambegaokar, in *Low Temperature Physics, LT9A*, edited by J. G. Daunt and D. O. Edwards (Plenum, New York, 1965).

[58] Y. Masuda and M. Hashimoto, J. Phys. Soc. Jpn. **31**, 1661 (1971).
[59] K. Kumagai *et al.*, in *Ternary Superconductors*, edited by G. K. Shenoy, B. D. Dunlap, and F. Y. Fradin (Elsevier, Amsterdam, 1981), p. 185.
[60] Y. Iwasa, H. Shimoda, T. T. M. Palstra, Y. Maniwa, O. Zhou, and T. Mitani, Phys. Rev. B **53**, R8836 (1996).
[61] C. M. Brown, K. Prassides, Y. Iwasa, and H. Shimoda, in *Recent Advances in the Chemistry and Physics of Fullerenes*, edited by K. M. Kadish and R. S. Ruoff (Electrochemical Society, Pennington, NJ, 1997), Vol. 4.
[62] K. Prassides, K. Tanigaki, and Y. Iwasa, Physica C **282**, 307 (1997).
[63] A. L. Fetter and P. C. Hohenberg, in *Superconductivity*, edited by R. D. Parks (Dekker, New York, 1969), Vol. 2, p. 817.
[64] Daniel S. Fisher, M. P. A. Fisher, and D. A. Huse, Phys. Rev. B **43**, 130 (1991).
[65] P. G. deGennes, *Superconductivity of Metals and Alloys* (Benjamin, New York, 1966).
[66] U. Brandt, W. Pesch, and L. Tewordt, Z. Phys. **201**, 209 (1967).
[67] U. Brandt, Phys. Lett. **27A**, 645 (1968).
[68] K. Maki in *Superconductivity* (Ref. 63), p. 1035.
[69] V. Ambegaokar and A. Griffin, Phys. Rev. **137**, A1151 (1965).
[70] A. Wasserman and M. Springford, Ann. Phys. (N.Y.) **45**, 471 (1996); M. Springford and A. Wasserman, J. Low Temp. Phys. **105**, 273 (1996).
[71] V. Ambegaokar, in *Superconductivity* (Ref. 48), p. 259.
[72] C. Caroli, P. G. deGennes, and J. Matricon, Phys. Lett. **9**, 307 (1964).
[73] M. Cyrot, Phys. Kondens. Mater. **3**, 374 (1965).
[74] F. Gygi and M. Schluter, Phys. Rev. B **43**, 7609 (1991).
[75] D. Rainer, J. A. Sauls, and D. Waxman, Phys. Rev. B **54**, 10 094 (1996).
[76] R. J. Watts-Tobin, L. Kramer, and W. Pesch, J. Low Temp. Phys. **17**, 71 (1974).
[77] W. Pesch and L. Kramer, J. Low Temp. Phys. **15**, 367 (1974); L. Kramer and W. Pesch, Z. Phys. **269**, 59 (1974).
[78] M. Ichioka, N. Hayashi, and K. Machida, Phys. Rev. B **55**, 6565 (1997).
[79] B. Pöttinger and U. Klein, Phys. Rev. Lett. **70**, 2806 (1993).
[80] B. S. Chandrasekhar, Appl. Phys. Lett. **1**, 7 (1962); A. M. Clogston, Phys. Rev. Lett. **9**, 266 (1962).
[81] D. Saint-James, E. J. Thomas, and G. Sarma, *Type-II Superconductivity* (Pergamon, Oxford, 1969).
[82] N. R. Werthamer, E. Helfand, and P. C. Hohenberg, Phys. Rev. **147**, 295 (1966).
[83] M. Cyrot, J. Phys. (Paris) **27**, 283 (1966).
[84] Y. Masuda and N. Okubo, J. Phys. Soc. Jpn. **26**, 309 (1969).
[85] D. Eppel, W. Pesch, and L. Tewordt, Z. Phys. **197**, 46 (1966); W. Pesch, Phys. Lett. **28A**, 71 (1968).
[86] B. G. Silbernagel, M. Weger, and J. E. Wernick, Phys. Rev. Lett. **17**, 384 (1966).
[87] I. B. Goldberg and M. Weger, J. Phys. Soc. Jpn. **24**, 1279 (1968).
[88] W. Fite II and A. G. Redfield, Phys. Rev. **162**, 358 (1967).
[89] L. Xing and Y-C. Chang, Phys. Rev. Lett. **73**, 488 (1994).
[90] E. Ehrenfreund *et al.*, Solid State Commun. **7**, 1333 (1969); L. N. Bulaevskii, N. N. Kolesnikov, I. F. Schegolev, and O. M. Vyaselev, Phys. Rev. Lett. **71**, 1891 (1993); C. H. Recchia, J. A. Martindale, C. H. Pennington, W. L. Hults, and J. L. Smith, *ibid.* **78**, 3543 (1997).
[91] A. Z. Genack and A. G. Redfield, Phys. Rev. Lett. **31**, 1204 (1973).
[92] *Colloque Ampère Proceedings*, edited by R. Blinc (North-Holland, Amsterdam, 1967).
[93] F. Y. Fradin, in *Nuclear and Electron Resonance Spectroscopies Applied to Materials Science*, edited by E. N. Kaufman and G. K. Shenoy (Elsevier, Amsterdam, 1981).
[94] T. L. Duty, J. H. Brewer, K. Chow, R. F. Kiefl, W. A. MacFarlane, G. D. Morris, J. W. Schneider, B. Hitti, R. Lichti, L. Brard, J. E. Fischer, A. B. Smith III, and R. M. Strongin, Hyperfine Interact. **86**, 789 (1994).
[95] W. A. MacFarlane, R. F. Kiefl, S. Dunsiger, J. E. Sonier, and J. E. Fischer, Phys. Rev. B **52**, R6995 (1995).
[96] E. J. Ansaldo, C. Niedermayer, and C. E. Stronach, Nature (London) **353**, 129 (1991).
[97] E. Holzschuh, Helv. Phys. Acta **54**, 552 (1981).
[98] E. J. Mele and S. C. Erwin, Phys. Rev. B **50**, 2150 (1994).
[99] J. Mizuki, M. Takai, H. Takahashi, N. Môri, K. Tanigaki, I. Hirosawa, and K. Prassides, Phys. Rev. B **50**, 3466 (1994).
[100] V. A. Stenger, C. H. Pennington, D. R. Buffinger, and R. P. Ziebarth, Phys. Rev. Lett. **74**, 1649 (1995).
[101] Y. Maniwa, T. Saito, K. Kume, K. Kikuchi, I. Ikemoto, S. Suzuki, Y. Achiba, I. Hirosawa, M. Kosaka, and K. Tanigaki, Phys. Rev. B **52**, R7054 (1995).
[102] R. Tycko, G. Dabbagh, M. J. Rosseinsky, D. W. Murphy, A. P. Ramirez, and R. M. Fleming, Phys. Rev. Lett. **68**, 1912 (1992).
[103] V. Jaccarino, in *Proceeding of the International School of Physics ''Enrico Fermi,'' XXXVII*, edited by W. Marshall (Academic, New York, 1967), p. 365.
[104] B. S. Shastry and E. Abrahams, Phys. Rev. Lett. **72**, 1933 (1994).
[105] J. A. Chakhalian *et al.*, Hyperfine Interact. **106**, 245 (1997).
[106] K. H. Chow, R. F. Kiefl, J. W. Schneider, B. Hitti, T. L. Ertle, R. L. Lichti, C. Schwab, R. C. Duvarney, S. R. Kreitzman, A. MacFarlane, and M. Senba, Phys. Rev. B **47**, 16 004 (1993).
[107] Y. J. Uemura, A. Keren, L. P. Le, G. M. Luke, B. J. Sternlieb, W. D. Wu, J. H. Brewer, R. L. Whetten, S. M. Huang, S. Lin, R. B. Kaner, F. Diederich, S. Donovan, G. Grüner, and K. Holczer, Nature (London) **352**, 605 (1991).
[108] Y. J. Uemura, A. Keren, L. P. Le, G. M. Luke, W. D. Wu, J. S. Tsai, K. Tanigaki, K. Holczer, S. Donovan, and R. L. Whetten, Physica C **235-240**, 2501 (1994).
[109] W. A. MacFarlane, R. F. Kiefl, K. Chow, S. Dunsinger, T. L. Duty, T. M. S. Johnston, J. W. Schneider, J. Sonier, L. Brard, R. M. Strongin, J. E. Fischer, and A. B. Smith III, Hyperfine Interact. **86**, 467 (1994).
[110] E. H. Brandt, Phys. Rev. B **37**, 2349 (1988).
[111] B. Pümpin, H. Keller, W. Kündig, W. Odermatt, I. M. Savić, J. W. Schneider, H. Simmler, P. Zimmermann, E. Kaldis, S. Rusiecki, Y. Maeno, and C. Rossel, Phys. Rev. B **42**, 8019 (1990).
[112] T. M. Riseman, J. H. Brewer, K. H. Chow, W. N. Hardy, R. F. Kiefl, S. R. Kreitzman, R. Liang, W. A. MacFarlane, P. Mendels, G. D. Morris, J. Rammer, J. W. Schneider, C. Niedermayer, and S. L. Lee, Phys. Rev. B **52**, 10 569 (1995).
[113] J. E. Sonier, M.Sc. thesis, University of British Columbia, 1994.
[114] J. R. Clem, J. Low Temp. Phys. **18**, 427 (1975).
[115] Z. Hao, J. R. Clem, M. W. McElfresh, L. Civale, A. P. Malozemoff, and F. Holtzberg, Phys. Rev. B **43**, 2844 (1991).
[116] A. Yaouanc, P. Dalmas de Réotier, and E. H. Brandt, Phys. Rev. B **55**, 11 107 (1997).

[117] J. E. Sonier, R. F. Kiefl, J. H. Brewer, D. A. Bonn, J. F. Carolan, K. H. Chow, P. Dosanjh, W. N. Hardy, Ruixing Liang, W. A. MacFarlane, P. Mendels, G. D. Morris, T. M. Riseman, and J. W. Schneider, Phys. Rev. Lett. **72**, 744 (1994).

[118] J. E. Sonier, J. H. Brewer, R. F. Kiefl, D. A. Bonn, S. R. Dunsiger, W. N. Hardy, R. Liang, W. A. MacFarlane, R. I. Miller, T. M. Riseman, D. R. Noakes, C. E. Stronach, and M. F. White, Jr., Phys. Rev. Lett. **79**, 2875 (1997).

[119] J. E. Sonier, R. F. Kiefl, J. H. Brewer, J. Chakhalian, S. R. Dunsiger, W. A. MacFarlane, R. I. Miller, A. Wong, G. M. Luke, and J. W. Brill, Phys. Rev. Lett. **79**, 1742 (1997).

[120] G. Zimmer, M. Mehring, F. Rachdi, and J. E. Fischer, Phys. Rev. B **54**, R3768 (1996).

[121] L. Degiorgi, P. Wachter, G. Grüner, S. M. Huang, J. Wiley, and R. B. Kaner, Phys. Rev. Lett. **69**, 2987 (1992).

[122] J. E. Sonier, R. F. Kiefl, J. H. Brewer, D. A. Bonn, S. R. Dunsiger, W. N. Hardy, R. Liang, W. A. MacFarlane, T. M. Riseman, D. R. Noakes, and C. E. Stronach, Phys. Rev. B **55**, 11 789 (1997).

[123] P. J. Hirschfeld and N. Goldenfeld, Phys. Rev. B **48**, 4219 (1993).

[124] C. Christides, D. A. Neumann, K. Prassides, J. R. D. Copley, J. J. Rush, M. J. Rosseinsky, D. W. Murphy, and R. C. Haddon, Phys. Rev. B **46**, 12 088 (1992).

[125] Z. Zhang, C. C. Chen, and C. M. Lieber, Science **254**, 1619 (1991).

[126] P. Jess, S. Behler, M. Bernasconi, V. Thommen-Geiser, H. P. Lang, M. Baenitz, K. Lüders, and H. J. Güntherodt, Physica C **235-240**, 2499 (1994).

[127] J. Ostrick (unpublished).

[128] S. K. Watson, K. Allen, D. W. Denlinger, and F. Hellman, Phys. Rev. B **55**, 3866 (1997).

[129] A. Yazdani, B. A. Jones, C. P. Lutz, M. F. Crommie, and D. M. Eigler, Science **275**, 1767 (1997).

[130] K. Tanigaki, I. Hirosawa, T. Manako, J. S. Tsai, J. Mizuki, and T. W. Ebbesen, Phys. Rev. B **49**, 12 307 (1994).